Direct observation of fluorescent proteins in gels: a rapid cost-efficient, and quantitative alternative to immunoblotting

Matthieu Sanial[1], Ryan Miled[1], Marine Alves[1], Sandra Claret[1], Nicolas Joly[1], Véronique Proux-Gillardeaux[1], Anne Plessis[1], Sébastien Léon[1,2]

Affiliations:

[1] : Université Paris Cité, CNRS, Institut Jacques Monod, F-75013, Paris, France.

[2] : Author for correspondence:

Sébastien Léon, PhD

Institut Jacques Monod

15 Rue Hélène Brion

75205 Paris cedex 13, France.

email: sebastien.leon@ijm.fr ; tel. +33 (0)1 57 27 80 57.

Running title:

In-gel fluorescence detection of fluorescent proteins as an alternative to immunoblotting

Abstract

The discovery of Green Fluorescent Protein (GFP) and its derivatives has revolutionized cell biology. These fluorescent proteins (FPs) have enabled the real-time observation of protein localization and dynamics within live cells. Applications of FP vary from monitoring gene/protein expression patterns, visualizing protein-protein interactions, measuring protein stability, assessing protein mobility and creating biosensors. The utility of FPs also extends to biochemical approaches through immunoblotting and proteomic analyses, aided by anti-FP antibodies and nanobodies. FPs are notoriously robust proteins with a tightly folded domain that confers a strong stability and a relative resistance to degradation and denaturation. In this study, we report that various green, orange and red FPs can be maintained in a native, fluorescent state during the entire process of protein sample extraction, incubation with sample buffer, loading and migration on SDS-PAGE with only minor adaptations of traditional protocols. This protocol results in the ability to detect and quantify in-gel fluorescence (IGF) of endogenously-expressed proteins tagged with FPs directly after migration, using standard fluorescence-imaging devices. This approach eliminates the need for antibodies and chemiluminescent reagents, as well as the time-consuming steps inherent in immunoblotting such as transfer onto a membrane and antibody incubations. Overall, IGF detection provides clearer data with less background interference, a sensitivity comparable or better to antibody-based detection, a better quantification and a broader dynamic range. After fluorescence imaging, gels can still be used for other applications such as total protein staining or immunoblotting if needed. It also expands possibilities by allowing the detection of FPs for which antibodies are not available. Our study explores the feasibility, limitations, and applications of IGF for detecting endogenously expressed proteins in cell extracts, providing insights into sample preparation, imaging conditions, and sensitivity optimizations, and potential applications such as co-immunoprecipitation experiments.

Introduction

The development of GFP as a tool to study protein localization and dynamics in live cells has been a revolution in the field of cell biology, as recognized by the Nobel prize in Chemistry awarded in 2008 to Osamu Shimomura, Martin Chalfie and Roger Tsien (Chalfie et al., 1994; Tsien, 1998). GFP and its derivatives, as well as other fluorescent proteins (FPs) isolated since then from other organisms with various properties (Lambert, 2019; Shaner et al., 2005), have become instrumental in many fields of biology. They allow to monitor protein expression and localization in live cells, and can be used as reporters of gene/protein expression patterns in organisms or tissues. Various techniques have been implemented using GFP and its variants to visualize protein-protein interactions in cells, through bimolecular fluorescence complementation (Hu and Kerppola, 2003; Romei and Boxer, 2019), or fluorescence resonance energy transfer (FRET, BRET) (Hochreiter et al., 2015). This also opened the way to the development of various probes and biosensors to report on the quantity and/or localization of ions, metabolites and other organic molecules in cells and tissues (Chandris et al., 2021; Wang et al., 2023; Zacharias et al., 2002). Diverse folding kinetics of FPs have been exploited to report on protein stability and half-life (fluorescent timers) (Khmelinskii et al., 2012; Subach et al., 2009; Terskikh et al., 2000). The fact that fluorescence bleaches upon intense illumination also provides a way to evaluate protein mobility and dynamics in live cells (Fluorescence Recovery after Photobleaching [FRAP] and Fluorescence Loss in Photobleaching [FLIP]) (White and Stelzer, 1999). Similarly, photo-activatable and photo-switchable FPs allow the study of distinct protein pools over time by activating or converting their fluorescence upon illumination (Wang et al., 2023). Following the development of robust anti-GFP antibodies and in particular of nanobodies (Rothbauer et al., 2006), GFP can also be used like any other epitope for protein detection by techniques ranging from immunoblotting to immunoprecipitation and proteomic analyses (Cristea et al., 2005; Rothbauer et al., 2008). Finally, the ability to express a GFP-binding protein (derived from a llama single chain antibody) in cells fused with cellular proteins provides a way to modify the subcellular localization and interactions of a GFP-tagged protein at will (Rothbauer et al., 2008).

Because of these many applications, GFP and other FPs are frequently used as protein tags in cell biology studies. An early step in the workflow consists in verifying the expression of an intact fusion protein in cells by immunoblotting. Immunoblotting is also required when GFP is used as any epitope to monitor the fusion protein's integrity, stability or post-translational modifications, or in interaction studies based on co-immunoprecipitations. Protein detection by immunoblotting involves primary antibodies and most generally a chemiluminescent reaction (ECL) using secondary antibodies coupled to an enzyme (horseradish peroxidase, HRP). Whereas this approach is considered to be more sensitive, HRP kinetics may interfere with the linearity of the signal vis-à-vis the amount of detected protein, a problem that may hinder the quantification of signals.

62 Over the past 20 years, fluorescent alternatives to chemiluminescence-based protein detection
63 were introduced, and the development of fluorescent dyes and the amelioration of fluorescence-
64 based imaging systems have allowed for a better sensitivity and better quantification of signals
65 (Eaton et al., 2014). Although initial systems focused on fluorescence detection at high wavelengths
66 (far-red and infrared, i.e. around 700 nm and above) to minimize background autofluorescence,
67 commercial imaging systems now allow the visualization of fluorescence at additional wavelengths
68 compatible with usual commercial fluorophores, eg. those used for immunofluorescence.
69 The versatility of these imaging systems is such that, in principle, the endogenous
70 fluorescence of the widely used FPs (eg. GFP) in extracts could be monitored directly in gels without
71 the need of transfer to membrane or the use of antibodies. SDS-PAGE involves denaturation of
72 protein samples at high temperatures in the presence of SDS and reducing agents prior to loading
73 onto a gel, procedures that are usually considered incompatible with the maintenance of FP
74 fluorescence in gel (Chew et al., 2009). Other types of fluorescent proteins, such as using Flavin-
75 binding FPs, bacteriophytochrome-based FPs, or bilirubin-binding FP (UnaG) can be used to detect
76 proteins *in vivo* or *in vitro* (Rodriguez et al., 2017; Shcherbakova et al., 2015), some of which can
77 be visualized in gel in the near-infrared from a fully-denatured extract in the presence of zinc acetate
78 (Berkelman and Lagarias, 1986; Stepanenko et al., 2022). However, this relies on less commonly
79 used fluorescent protein tags, with spectral properties that are not always available in classical
80 fluorescence microscopy setup, usually preventing a combined use of these tags for imaging and
81 biochemical studies.
82 A few studies have reported the observation of GFP-fluorescence in gels, but these approaches
83 require the use of native PAGE (Nemec et al., 2017), which has drawbacks compared to regular,
84 denaturing SDS-PAGE. On the other hand, GFP and FPs in general are known to be tightly folded
85 and more resistant to denaturation than most proteins (Saeed and Ashraf, 2009; Ward, 2005). For
86 example, a few studies exploited the ability of GFP to resist the adverse conditions of SDS-PAGE to
87 run protein overexpression screens in *Escherichia coli* or other cell types (Aoki et al., 1996; Bird et
88 al., 2015; Bomholt et al., 2013; Drew et al., 2006; Geertsma et al., 2008; Krasnoselska et al., 2021;
89 Madani et al., 2021; Muller-Lucks et al., 2012; Newstead et al., 2007), or on recombinantly expressed
90 or purified proteins *in vitro* (Aoki et al., 1996; Campbell et al., 2002; Donate-Macian et al., 2019;
91 Koldenkova et al., 2015; Nakatani et al., 2019; Weinberger Ii and Lennon, 2021; Yanushevich et al.,
92 2002).
93 The development and popularity of fluorescence imaging devices is likely to lead to a
94 generalization of the use of FPs for direct visualization of in-gel fluorescence (IGF). Accordingly, a
95 recent study used this method for easy detection of FP-tagged proteins in protein extracts of cell
96 culture (Ruan et al., 2024).
97 In this study, we document that in-gel fluorescence (IGF) detection is a rapid and cost-effective
98 alternative to immunoblotting to visualize FP-tagged proteins expressed at endogenous levels in cell
99 extracts. IGF avoids the time-consuming process of transfer to a membrane, incubations with

antibodies and washes, with substantial improvements of the cost of the experiment as this does not require primary nor secondary antibodies, membranes, or chemiluminescence substrates, and of the quality of the data (less background and higher dynamic range). We describe the conditions of use and limitations of various GFPs and RFPs for IGF, as well as sample preparation, imaging conditions, sensitivity and possible applications.

106 # Results

107 ## The fluorescence of endogenously yeGFP-tagged proteins can be
108 visualized from cell extracts in SDS-PAGE gel after migration

109 To know whether we can detect GFP fluorescence from endogenously expressed proteins in
110 total protein extracts, we tagged two yeast genes (*BMH1*, encoding a 14-3-3 protein) or *HXK1*,
111 encoding hexokinase 1) at their endogenous locus with yeGFP, a yeast codon-optimized GFP
112 (Cormack et al., 1997) which also harbors two mutations (S65G, S72A - a.k.a. "GFPmut 3", Cormack
113 et al., 1996) selected to increase GFP fluorescence (ID on FPBase https://www.fpbase.org :
114 A2OWC, Lambert, 2019). yeGFP is often used for fluorescent tagging as it is incorporated into a
115 toolbox for PCR-based tagging of yeast genes at their endogenous genetic locus (Janke et al.,
116 2004). Exponentially growing cells (5 OD equivalents) were lysed with glass beads at 4°C in 100 µL
117 native lysis buffer (containing Tris-HCl, Triton X-100 and NaCl; see Material and Methods for more
118 details). 4X Laemmli sample buffer (Bio-Rad, containing lithium dodecyl sulfate [LDS] and
119 dithiothreitol [DTT]) was then added to the lysates (1X final), and samples were then incubated at
120 30°C or 95°C for 5 min, before loading on commercial precast TGX (Tris-Glycine eXtended) gels,
121 and run in Tris-Glycine-SDS (TGS) buffer. After migration, the gel was imaged with gel-imaging
122 devices whose excitation/emission wavelengths were compatible with the observation of green
123 fluorescent proteins (ChemiDoc MP, Bio-Rad: 460-490/518-546 nm; and Typhoon, Cytiva: 488/505-
124 545 nm) (**Figure S1**). The gels displayed a green fluorescent signal at the size of the tagged proteins,
125 as revealed by immunoblotting with anti-GFP antibodies after transfer of the same gel to a
126 membrane (**Figure 1A**). Thus, at least some GFP molecules remained fluorescent throughout
127 sample preparation and gel migration process. Noteworthy, other lysis buffers were tested and also
128 allowed the maintenance of GFP fluorescence (see Material and Methods for more details). On a
129 side note, we observed that gel exposure to UV-light (such as during total protein labeling with a
130 trihalo compound, eg. "Stain-Free" technology from Bio-Rad: 45 sec exposure at 300-400 nm)
131 partially bleached the GFP fluorescence signal (**Figure S2**). Thus, this labeling should preferentially
132 be performed after visualizing the GFP signal, especially if the signal is weak. Finally, as expected,
133 GFP was no longer fluorescent when samples were denatured at 95°C instead of 30°C, or when
134 extracts were prepared from cells precipitated with TCA in which proteins are fully denatured (**Figure
135 1A**).

136 Whereas these mild denaturing conditions allow the detection of in-gel fluorescence, two
137 important points should be noted. First, the lower level of denaturation can impact on the migration
138 of the GFP-tagged protein. At 30°C, Bmh1-yeGFP and Hxk1-yeGFP migrated faster than when
139 samples were heated at 95°C or precipitated with TCA, as determined after transfer and
140 immunoblotting with anti-GFP antibodies (**Figure 1A**). In-gel fluorescence detection systematically
141 correlated with the presence of the fast-migrating band, suggesting it may correspond to a folded

142 species of yeGFP, in agreement with previous observations (Aoki et al., 1996). To address this point,
143 proteins were transferred onto a nitrocellulose membrane in classical conditions (liquid transfer), and
144 immunoblotted with anti-GFP antibodies. Bmh1-yeGFP fluorescence signal could be detected on
145 the nitrocellulose membrane even after transfer and incubation with antibodies, allowing the
146 sequential observation of yeGFP fluorescence and antibody-based labeling during the same
147 acquisition. This revealed that the yeGFP fluorescence signal precisely overlaid with the fast-
148 migrating band detected with the anti-GFP antibody (**Figure 1B**). Thus, yeGFP remains mostly
149 folded in these mild denaturation conditions allowing in-gel fluorescence observation, but can also
150 cause a variation in the apparent molecular weight of yeGFP-tagged proteins as compared to
151 denatured proteins.

152 A second aspect that should be considered when using low denaturing conditions is that various
153 antibodies may recognize folded and denatured fluorescent proteins with different affinities. For
154 instance, anti-GFP antibodies may display a greater affinity towards folded or unfolded GFP, leading
155 to potential artifacts during quantification of the signal (**Figure S3A**). This could be circumvented by
156 denaturing proteins directly on the membrane after transfer (**Figure S3B**, see Material and Methods).

157 Comparison of GFP(S65T), yeGFP and EGFP for in-gel fluorescence 158 visualization

159 Following the development of tools for tagging of yeast genes with various tags by homologous
160 recombination (Longtine et al., 1998; Wach et al., 1997), Huh et al. generated a collection of yeast
161 strains which is widely used by the community and in which most genes are individually tagged with
162 GFP(S65T) (Huh et al., 2003) (FPBase ID: B6J33). To evaluate whether strains from this collection
163 are suitable for in-gel fluorescence detection, we retrieved the Bmh1-GFP(S65T) strain and
164 subjected it to the same analysis. A fluorescent signal was detected in the gel when samples were
165 incubated at 30°C, but not 95°C (**Figure 2A**). When compared to the signal obtained when tagging
166 the same protein with yeGFP, the fluorescent signal observed with GFP(S65T) was weaker,
167 probably because GFP(S65T) was less robust and more prone to denaturation. Indeed, a large
168 fraction of the Bmh1-GFP(S65T) protein pool was denatured even when incubated at 30°C prior to
169 gel loading, as judged by the migration pattern revealed with anti-GFP antibodies and antibodies
170 directed to the proteins of interest (**Figure 2A**). Thus, GFP(S65T) is subject to a partial denaturation
171 even in conditions which otherwise preserve yeGFP fluorescence. This was confirmed when
172 comparing the staining of Hxk1-GFP(S65T) with that of Hxk1-yeGFP (**Figure 2A**). In conclusion,
173 fusions with GFP(S65T) (including those from the GFP collection, Huh et al., 2003) are not the best-
174 suited to detect in-gel fluorescence in our conditions.

175 We also tested another commonly used GFP variant, EGFP, which derives from the original
176 avGFP and carries mutations F64L and S65T (a.k.a. “GFPmut 1”, FPBase ID: R9NL8, Cormack et
177 al., 1996). This variant is also commonly used for the tagging of yeast genes at their endogenous
178 genetic locus (Janke et al., 2004) and is widely used in other eukaryotic organisms, notably through

179 their availability in the pEGFP-N1/pEGFP-C1 plasmids for expression in mammalian cells. The
180 signals obtained with EGFP were comparable to those obtained for yeGFP, making it appropriate
181 for visualization of IGF (**Figure 2B**).

182 In-gel fluorescence detection of proteins tagged with mNeonGreen and 183 superfolder GFP

184 We next tested the suitability of more recently developed green-fluorescent proteins for IGF
185 detection (**Figure 3**). For comparative purposes, the same protein that we used for the initial variants
186 tested, Bmh1, was tagged with the brighter dLanYFP-derivative, mNeonGreen (FPBase ID: ZRKRV,
187 Shaner et al., 2013) or with superfolder GFP (sfGFP), a tightly folded GFP which is even more
188 resistant to denaturation than traditional GFP (FPBase ID: B4SOW, Pedelacq et al., 2006).
189 In all cases, a fluorescent signal was detected in the gel when samples were incubated at 30°C
190 prior to loading (**Figure 3**). Various fluorescence intensities were observed, with the strongest signal
191 obtained for Bmh1-yeGFP. However, these variations could be due to (i) the spectral properties of
192 these fluorescent proteins which may not appropriately match the imaging systems used for their
193 detection, (ii) the ability of these fluorescent proteins to endure the sample preparation conditions
194 and SDS-PAGE protocol, and (iii) an effect of the tag on the expression level of the tagged protein
195 (**Figure 3**). Indeed, in our experiments, Bmh1-yeGFP was more highly expressed than Bmh1-
196 mNeonGreen or Bmh1-sfGFP, as determined by immunoblotting these proteins with anti-Bmh1
197 antibodies. We hypothesized that this lower level of expression might be due to the fact that only
198 Bmh1-yeGFP is codon-optimized for expression in yeast. However, optimizing codon usage for
199 mNeonGreen expression in yeast (ymNeonGreen) neither led to an increase in protein expression
200 nor in IGF signal (**Figure S4**). This hypothesis remains open for sfGFP, as we did not test
201 optimization of codon usage for this FP.
202 The loss of IGF signal upon denaturation at 95°C was accompanied by a change in the migration
203 pattern as revealed by western blotting using anti-Bmh1 antibodies, with only one band present at a
204 higher apparent molecular weight, corresponding to the non-fluorescent species. An intermediate
205 situation was observed upon denaturation at 50°C, with a decrease in Bmh1-mNeonGreen IGF,
206 unlike what was observed for Bmh1-yeGFP or sfGFP (**Figure 3**). Accordingly, by immunoblotting,
207 treatment of samples at 50°C led to an almost full conversion of Bmh1-mNeonGreen from the native
208 to the denatured form, which was less pronounced for Bmh1-yeGFP. Thus, mNeonGreen is
209 amenable to IGF detection but is less heat-stable than other green FPs. In contrast, Bmh1-sfGFP
210 migration was unaffected at 50°C compared to 30°C, highlighting the stronger heat-stability of this
211 fluorescent variant. Overall, we conclude that sfGFP and EGFP (see **Figure 2B**) are more resistant
212 to heat-induced denaturation than yeGFP, GFP(S65T) and mNeonGreen.
213 These observations led us to quantify the heat-stability of fluorescence of the most robust green
214 FPs, which could be helpful for applications in which samples must be incubated at temperatures
215 higher than 30°C. We determined in-gel fluorescence as a function of the denaturation temperature

216 (**Figure 4**). In-gel fluorescence of Bmh1-sfGFP was unaltered until reaching 59°C, whereas Bmh1-
217 yeGFP fluorescence decreased starting at 54°C (**Figure 4A, C-D**). The temperature at which 50%
218 of the signal is still present was 67°C for sfGFP and 59°C for yeGFP. Interestingly, EGFP behaved
219 similarly to sfGFP (**Figure 4B, D**). The only additional gain of tagging with sfGFP over the widely
220 used EGFP is that it migrates almost exclusively as a single band at low denaturing temperatures
221 (30°C). Again, denaturation of all green FP-tagged Bmh1 was accompanied by a decrease in its
222 mobility on gels, which could clearly be visualized using anti-Bmh1 antibodies (**Figure 4, A-C**).
223 Altogether, these results allow us to reach the following conclusions. First, Bmh1-yeGFP and
224 Bmh1-EGFP give a strong IGF signal that, in our experiments, could be attributed to a higher
225 expression level coupled to a relatively high resistance to denaturation, especially in the case of
226 EGFP. Indeed, EGFP was as resistant as sfGFP to heat-induced denaturation in our conditions.
227 Second, despite being more sensitive to the conditions of extraction and imaging, mNeonGreen in-
228 gel fluorescence can still be used at low denaturation temperatures, which can avoid the purchase
229 of specific antibodies – indeed, mNeonGreen shares only 25% identity with the traditional avGFP
230 and is not recognized by anti-GFP antibodies. Finally, care should be taken regarding the expression
231 level of the tagged protein which, despite tagging at the endogenous genetic locus, can lead to
232 strong variations in expression depending on which FP was used for tagging (see **Figure 3**).

233 In-gel fluorescence of red and orange fluorescent proteins

234 We aimed at expanding our observations to other, non-green fluorescent proteins. We could
235 not test blue-fluorescent proteins because none of the commonly-used imaging devices (Chemidoc
236 MP and Typhoon) provide filters compatible with the excitation/emission spectra of blue-fluorescent
237 proteins. However, these experiments were possible for red-fluorescent proteins. We tagged Bmh1
238 with the widely used fluorescent protein mCherry, a monomeric DsRed derivative with many
239 advantages such as high photostability, faster maturation and high pH-stability (FPBase ID: ZERB6,
240 Shaner et al., 2004). We also fused Bmh1 with mRuby2, a bright derivative of eqFP611 (FPBase ID:
241 8MJ78, Lam et al., 2012) , and with TagRFP-T, which derives from eqFP578 (Merzlyak et al., 2007)
242 with enhanced photostability (FPBase ID: LF3LJ, Shaner et al., 2008). Finally, we also tested fusion
243 of Bmh1 with mKO-κ, a derivative of the monomeric orange fluorescent protein mKO (Karasawa et
244 al., 2004) further mutagenized for faster maturation (FPBase ID: HMK8R, Tsutsui et al., 2008)
245 because of its spectral properties that make it more appropriate for detection by the Chemidoc MP
246 (**Figure S5**). Protein extracts were run on SDS-PAGE and in-gel fluorescence was observed at
247 excitation/emission wavelengths of 532/550-800nm (Typhoon) or 520-545/577-613nm (ChemiDoc
248 MP). All samples gave a fluorescent signal in gel (**Figure 5A**). Fluorescence signals were globally
249 stronger when using a long-pass filter on the Typhoon (550-800nm), which collects more
250 fluorescence signals than the narrower filter present on the Chemidoc MP (577-613nm) (**Figure S5**).
251 The strongest fluorescence signals were obtained for Bmh1 mKO-κ and Bmh1-mCherry, whereas
252 Bmh1-TagRFP-T gave the weakest signal. Immunoblotting using anti-Bmh1 antibodies revealed

253 migration patterns comparable to those obtained for green fluorescent proteins: a faster-migrating
254 band corresponded to the fluorescent species, whereas the slower migrating form corresponded to
255 the denatured pool. The ratio of fluorescent over denatured proteins was higher for mCherry,
256 although a minor denatured pool was already present in mild denaturing conditions. Notably, the
257 fluorescent pool of Bmh1-mRuby2 and Bmh1 mKO-κ migrated much faster than any other FP-tagged
258 Bmh1 protein, with a decrease of about 15 kDa in apparent MW compared to the denatured version.
259 Bmh1-mKO-κ was the best detected red fluorescent protein on the Chemidoc MP (**Figure 5A**), likely
260 because of its spectral properties (**Figure S5**) which were more appropriate for detection on this
261 device; however, a strong signal was also observed for Bmh1-mCh. Altogether, our conclusions are
262 that (i) mild denaturation conditions are compatible with IGF of orange and red FPs, with mCherry
263 and mKO-κ being the best tags in our hands, with a stronger signal and resistance to heat-induced
264 denaturation; (ii) IGF allows the visualization of proteins tagged with orange and red FPs originating
265 from various organisms without the need to purchase specific antibodies; (iii) tagging of proteins with
266 orange and red FPs can lead to significant changes in the apparent molecular weight of the fusion
267 proteins in mild denaturing conditions.

268 Because of the higher signal intensity provided by mKO-κ and mCherry, and the fact that the
269 latter is a widely used FP, we then evaluated the resistance of Bmh1-mCh and Bmh1-mKO-κ to
270 temperature-induced denaturation (**Figure 5, B-C**). Both mKO-κ and mCherry fluorescence was
271 maintained at up to 60°C, with 50% of the signal still being present at 79°C (for mCherry) or 82°C
272 (for mKO-κ). Thus, of all FPs tested (including green FPs), mCherry and mKO-κ are the most
273 resistant to denaturation and are therefore perfectly appropriate for IGF signal detection.

274 Linearity of the signal and sensitivity of IGF compared to antibody-based 275 detection

276 Having established the capacity to detect fluorescence of numerous FPs in gels, we then turned
277 to studying the linearity of the signal and the sensitivity of this approach compared to the traditional
278 immunoblotting approach. When serial dilutions of Bmh1-yeGFP samples were initially assayed, we
279 discovered that the simple dilution of the protein lysate in Laemmli buffer (containing SDS and DTT)
280 was sufficient to promote FP denaturation, as determined by examining the migration profile using
281 anti–Bmh1 antibodies. This was likely a consequence of an increase in the detergent/protein ratio,
282 as previously observed (Xu and Keiderling, 2004) (**Figure S6A**). To circumvent this problem, we
283 repeated the experiment using a non-denaturing sample buffer for dilutions of the sample (Laemmli
284 buffer without LDS). Under these conditions, protein fluorescence was maintained in spite of the
285 dilution (**Figure 6**).

286 In-gel fluorescence was compared to the signal obtained using primary anti-GFP antibodies
287 followed by secondary antibodies coupled to either horseradish peroxidase (HRP) for
288 chemiluminescent detection (**Figure 6A**) or to a fluorescent dye (**Figure 6B**). Overall, IGF detection
289 was better in sensitivity to chemiluminescent or antibody-based fluorescence detection in our

290 conditions. Overall, we found the IGF signal to more closely follow a linear plot than antibody-based
291 signals, over a range of 320-fold (**Figure 6B**). The linearity of signal intensity as a function of protein
292 dilution was confirmed for all FPs we tested, including mCherry and mKO-κ (**Figure S7**). Thus, we
293 conclude that IGF detection is more reliable and sensitive than antibody-based detection.

294 Our observations above (**Figure S6A**) suggested that sample dilution in Laemmli buffer
295 compromises the integrity of GFP. Although we observed that this could be circumvented by the use
296 of detergent-free Laemmli buffer (**Figure 6**), we sought to find conditions in which sample dilution
297 would maintain FP integrity despite the presence of detergent (**Figure S6B**). First, we observed that
298 dilution of the protein lysate in native lysis buffer (Tris-HCl 100 mM pH 8.0, NaCl 0.15 M, Glycerol
299 5%, Triton X-100 0.5 %) instead of water (**Figure S6B**) led to a protection of fluorescence, as
300 determined both by IGF detection and the observation of native/denatured species by
301 immunoblotting (**Figure S6C**). This result could partially be attributed to the presence of NaCl in the
302 native lysis buffer, which preserved fluorescence in itself (**Figure S6C**). Moreover, increasing the pH
303 to 8.0 or above was sufficient to protect fluorescence at low protein concentrations (**Figure S6D**),
304 allowing IGF detection even for diluted protein samples. We conclude that increasing the sample pH
305 to pH 8.0 protects GFP denaturation in diluted samples.

306 IGF detection on various endogenously-tagged proteins from yeast

307 We then aimed at detecting various proteins expressed at their endogenous level to address
308 several questions. For these experiments, proteins were tagged with EGFP given its superior
309 performances (see **Figure 2B**).

310 First, because Bmh1 and Hxk1 are rather abundant proteins (65,000 and 41,000 copies/cell,
311 respectively; Ho et al., 2018), we determined IGF signals for proteins of lower abundance. IGF signal
312 were obtained from proteins of abundance ranging from 736 to 65471 copies/cell (Ho et al., 2018)
313 and originating from various subcellular locations (cytosol, nucleus, mitochondria, microtubules,
314 plasma membrane, ER membrane) (**Figure 7A**). All proteins gave a signal at the expected size
315 (**Figure 7B**), suggesting that IGF is applicable to proteins expressed at a low level. IGF signal
316 intensity was then correlated with the published abundance originating from multiple studies (Ho et
317 al., 2018) (**Figure 7C**). This revealed a good correlation between our IGF quantitation and these
318 data, regardless of the type of experiments used for quantitation (quantitative proteomics, western
319 blotting or confocal microscopy) (**Figure S8A**). It was also clear that in our conditions, IGF led to an
320 overall better quality of detection than antibody-based chemiluminescence (**Figure S8B**).

321 Second, to check whether our conditions were sufficient to disrupt protein-protein interactions
322 at the low denaturation temperatures we use, we tested proteins engaged in large protein
323 complexes. Among the proteins we tested, several belonged to large complexes, such as RNA
324 polymerase I (Rpa12), proteasome (Pre6), or mitochondrial ribosome (mRpl25). All of these
325 migrated at the expected size (**Figure 7B**), with only one band being detected, suggesting disruption
326 of protein-protein interactions even in our mild denaturation conditions.

327 Third, we also looked at proteins from various subcellular compartments as well as membrane
328 proteins. The plasma membrane glucose transporter Hxt5 and the ER membrane-localized P-type
329 ATPase Spf1 migrated at the appropriate size, although a doublet was observed for Spf1 as
330 previously reported (Corradi et al., 2012; Hovsepian et al., 2017). The plasma membrane protein
331 Ina1 also migrated as a diffuse band at the expected size given its high glycosylation, as previously
332 reported (Laussel et al., 2022).
333 Altogether, our results show that IGF allows to visualize soluble and membrane proteins from
334 various compartments, even when expressed at a modest level, and that the mild denaturation
335 conditions are sufficient to denature high-order protein complexes.
336

337 Use of IGF for the detection of FP-tagged proteins interaction by co-
338 immunoprecipitation and compatibility with fluorescent SNAP-tagging

339 We sought to exploit the power of IGF detection in a situation in which two fluorescent proteins
340 must be detected. Protein-protein interactions can be studied by the co-expression of tagged
341 proteins and immunoprecipitation of one partner to reveal the presence of the potential partner in
342 the immunoprecipitate. As a case study, we studied the interaction between the yeast 14-3-3
343 proteins Bmh1 and Bmh2, which are known to heterodimerize *in vivo* (Chaudhri et al., 2003). Lysates
344 of yeast expressing Bmh1-yeGFP and Bmh2-ymCh (a yeast codon–optimized version of mCherry,
345 see Material and Methods) were subjected to immunoprecipitation using nanobodies-based traps.
346 Similar to our observations on diluted samples (section above), we realized that immunoprecipitates
347 of FP proteins were denatured in the presence of Laemmli buffer, likely because of the low protein
348 concentration in these samples. Based on our findings above (**Figure S6**), immunoprecipitates were
349 resuspended in Laemmli buffer at pH 8.0 before loading, and samples were migrated on SDS-PAGE
350 and imaged for IGF. In both cases (GFP-trap: **Figure 8A**; RFP-trap: **Figure 8B**), IGF detection
351 allowed visualization of both the bait and the prey on the same gel after exposure to the appropriate
352 wavelengths, within minutes after uncasting the gel. One limitation was a bleed-through of intense
353 green fluorescence signals in the red channel, which was notably observed using the Chemidoc
354 (**Figure S9**) but also using the Typhoon to a limited extent (**Figure 8A**). Thus, when looking at
355 proteins tagged in both channels, the size of the green fluorescence-tagged protein should be
356 different from that of the mCherry-tagged protein, and appropriate negative controls (samples
357 without the GFP-tagged protein) should be included to determine the specificity of the signal.
358 Because IGF is a fluorescence-based method, we also examined its compatibility with other
359 approaches such as SNAP-tagging which allows a direct fluorescence-based detection and
360 quantification of tagged protein in gel after electrophoresis (Tirat et al., 2006). A strain expressing
361 Reg1-SNAP, tagged at its endogenous locus, was transformed with a plasmid expressing an
362 mCherry-tagged protein (Snf4) under the control of its endogenous promoter. Total extracts were

363 made in native conditions and SNAP fluorescence labeling was made after lysis using the SNAP-
364 surface Alexa Fluor 647 dye which fluoresces in the far-red channel. This allowed detection of both
365 mCh-tagged proteins and SNAP-tagged Reg1 in the gel after migration (**Figure 8C**). Therefore, IGF
366 is compatible with SNAP-tagging protocols, further extending its abilities for in-gel quantitation of
367 expression of multiple proteins.

368 ## Use of IGF in cell extracts from other organisms

369 Although IGF detection is based on endogenous FP fluorescence and thus should not be
370 affected by the cellular context in which these proteins are expressed, we tested the use of this
371 technique in other eukaryotic systems, including Drosophila cells or tissues (**Figure 9, A-B**), MDCK
372 cells (**Figure 9C**) and *Caenorhabditis elegans* whole organisms (**Figure 9D**). Protein extracts were
373 prepared from FP-expressing cells in native conditions, resuspended in Laemmli buffer and samples
374 were loaded on SDS-PAGE gels (see Material and Methods). Overall, only minor adaptations to
375 current protein extraction protocols were made, and in all cases, IGF was observed, indicating the
376 applicability of IGF detection to the analysis of protein lysates from other organisms. In particular,
377 detection of the EGFP-tagged plasma membrane transducer Smoothened (SMO), which is
378 phosphorylated in response to Hedgehog (Jia et al., 2004) shows that IGF detection can be used to
379 study membrane proteins and post-translational modifications. In the case of total extracts from *C.*
380 *elegans* worms, we could detect GFP and mCherry fluorescence signals, however, we observed the
381 presence of non-specific fluorescent signals in the green channel that may complicate the readout
382 of IGF. First, autofluorescence of *C. elegans* animals was previously reported (Pincus et al., 2016),
383 and using red fluorescent proteins would avoid this problem. Second, we propose additional ways
384 to circumvent this problem. A band migrating just below the 70-kDa marker appeared in lysates from
385 WT animals which did not express any FP construct (**Figure 9D**), but this band disappeared upon
386 denaturation at 50°C. A fluorescent smear of unknown origin was also observed at around 250 kDa
387 (**Figure S10A**), which resisted the denaturation at 50°C. However, this smear was not visible when
388 running the samples on homemade gels compared to commercial, pre-cast gels (**Figure S10B**),
389 probably because this fluorescent material did not migrate into the resolving gel. Whereas these
390 observations provide ways to circumvent the non-specific green fluorescence observed in *C.*
391 *elegans*, it remains that care should be taken when setting up IGF detection in other material,
392 including the use of negative, non-FP-tagged extracts to ensure the specificity of the signal.
393
394

395 # Discussion

396 Our study introduces in-gel fluorescence (IGF) detection as a rapid and cost-effective
397 alternative to traditional immunoblotting for visualizing fluorescent protein (FPs) signals in cell
398 extracts from yeast and other organisms, with minor adaptations of current protocols. The key points
399 resulting from our observations and optimizations are summarized in **Figure 10.**

400 Our work builds on the widespread use of FPs, particularly green and red fluorescent proteins
401 and their derivatives, as powerful tools in cell biology. GFP, originally developed as a live-cell
402 imaging marker, has since become key for various applications, including the monitoring of protein
403 expression and as a proteomic tool. Immunoblotting has traditionally been the method of choice to
404 visualize and quantify the expression of FP-tagged proteins. However, it comes with drawbacks, as
405 this is a time-consuming experiment with a substantial cost due to the reagents required, and is not
406 optimal for quantifications compared to fluorescence-based approaches. Here, we propose IGF
407 detection as a fast, easy and efficient alternative to this technique.

408 Our study offers a comprehensive examination of IGF detection as an innovative tool for
409 protein detection after SDS-PAGE. We provide a systematic comparison of a number of widely used
410 FPs. Our evaluation considered key parameters such as fluorescence intensity, heat-stability, and
411 their overall suitability for IGF detection in the context of standard SDS-PAGE protocols and
412 accessible imaging devices. Importantly, this technique can be performed without major adaptation
413 of classical protocols except that protein denaturation should be carried out at low temperatures.

414 Overall, IGF detection is also a cost-effective method. This technique eliminates the need for
415 specific antibodies, which may even not be available in the case of less conventional FPs, as well
416 as nitrocellulose membrane or ECL reagents. This makes it an attractive option for labs that operate
417 under budget constraints. Because the observation is done directly from the gel after migration with
418 no additional steps, problems frequently observed with immunoblotting can be avoided, such as
419 heterogeneity of protein transfer, uneven antibody deposition, stains, and uneven ECL spreading on
420 the membrane.

421 Moreover, IGF is a time-saving technique, bypassing the need for protein transfer and
422 blotting/washing steps, as the proteins of interest can be visualized immediately after migration. For
423 example, we were able to use this technique to quickly screen for GFP-containing clones directly on
424 lysates from colonies after transformation (See Material and Methods). This complementary
425 approach to PCR-based screening allows to quickly monitor protein expression and size in multiple
426 clones. The advantages of IGF detection are even more appealing in the case of co-
427 immunoprecipitations of two fluorescent proteins, since both the prey and the bait can be visualized
428 within minutes after migration, without interference of primary antibody/secondary antibody
429 recognition which can sometimes hinder signal analysis and quantification.

430 Normalization of the obtained IGF signal with respect to total proteins can be achieved without
431 transfer and immunoblotting of loading controls by several means. This can involve commercial

432 fluorescence-based approaches for total protein detection, after sample labeling (eg. Amersham
433 QuickStain kit [Cytiva] or No-Stain™ protein labeling kit [Invitrogen]), or directly in gel (Stain-Free
434 gels [Bio-Rad]). Also, after IGF imaging, a regular Coomassie staining of the gel can be reliably
435 quantified in the near-infrared wavelengths (**Figure 9B**) (Butt and Coorssen, 2013).

436 Another key advantage of IGF detection is its versatility. All fluorescent proteins tested gave
437 a fluorescent signal in gels, which is advantageous notably in the case of FPs for which antibodies
438 are not yet available. However, not all FPs perform equally under all conditions. The results show
439 variations in the efficiency of IGF detection, emphasizing the need to consider both the FP's
440 fluorescence properties and its resistance to denaturation. Our findings demonstrate that EGFP and
441 sfGFP, in particular, display strong in-gel signals and good resistance to denaturation. These
442 features make them prime candidates for IGF applications. Moreover, mCherry and mKO-κ stand
443 out for their exceptional heat-stability, maintaining their fluorescence even at relatively high
444 denaturing temperatures. This expands the possibilities of IGF detection to proteins that require
445 higher denaturation temperatures (such as proteins forming dimers or assembled in tight
446 complexes). In all cases, though, the intensity of the signal and the ability to specifically detect a
447 fluorophore depend on the available filters on the imaging systems, which were sometimes limiting
448 (especially in the case of mCherry) and could lead to bleed-through of signals when visualizing
449 green- and red-tagged proteins in the same sample.

450 Since fluorescent signals originate from the protein itself, the IGF detection method reduces
451 potential biases that can be encountered after using primary and secondary antibodies. Like all
452 fluorescence detection protocols, signal detection does not depend on a chemiluminescence
453 enzymatic reaction, which imposes kinetic constraints and whose activity can vary depending on
454 substrate accessibility. Depending on the antibody used, and thanks to the constant improvement in
455 the sensitivity of imaging devices, we found that IGF detection could outperform antibody-based
456 chemiluminescent detection, and the signal was globally more linear with respect to protein
457 concentration. This technique also allowed the detection of endogenous proteins with low
458 abundance. Moreover, changing acquisition settings may increase sensitivity, with less background
459 than observed with chemiluminescence.

460 However, like all techniques, IGF has its limitations. First, this technique relies on a mild
461 denaturation of proteins, which is not compatible with harsh treatments such as TCA precipitation,
462 which is often used to prepare yeast lysates. Whereas native lysate preparation may be more
463 complex than a simple TCA precipitation, it does not require more material and overall this protocol
464 remains faster considering that signals can be monitored immediately after migration. Moreover, our
465 protocol is compatible with regular lysate preparation from mammalian cells which is often made in
466 native conditions. Second, denaturation is performed at lower temperatures than usually performed
467 in classical protocols. We demonstrated that this was sufficient to separate proteins from higher-
468 order complexes (proteasome, mitochondrial ribosomes, RNA polymerase I) suggesting no apparent
469 drawbacks at this level. However, the tagged proteins themselves may also be partially resistant to

denaturation at the low temperatures used for IGF, which would lead to more than one fluorescent bands. This should be examined when setting up IGF for the first time on a given protein. Moreover, depending on the FP used for tagging, proteins treated in mild denaturation conditions can migrate as 2 discrete bands corresponding to the fluorescent and denatured forms of the FP. The apparent molecular weight of FP-tagged proteins is usually lower than under classical denaturation conditions, with up to 15-kDa difference with the denatured form in the case of mRuby2 or mKO- κ. Determining which temperature is best suited for a given FP may require setting up the conditions on a protein for which an antibody is available, so as to evaluate the extent of denaturation. This is an important step as this could preclude its use for absolute quantifications. The use of the most denaturation-resistant fluorescent proteins, such as sfGFP, mCherry or mKO-κ would be advised for these applications. Although IGF was compatible with a range of lysis buffers, it is also possible that the composition of the lysis buffer in which proteins are resuspended may alter overall fluorescence, depending on the abilities of FPs to remain folded and fluorescent in these conditions. It should be noted that we did not systematically analyze whether the linker region between the protein of interest and the fluorescence protein influenced IGF signal and FP denaturation. Finally, antibodies may recognize denatured and non-denatured forms of the FPs with different affinities. While these factors do not diminish the value of IGF, they highlight the need for appropriate controls when setting up IGF for protein detection.

The method's simplicity, cost-effectiveness, reliability and compatibility with existing FPs and current protocols (including co-immunoprecipitation and SNAP-tagging) make IGF detection an attractive alternative to immunoblotting which can greatly benefit research in a range of fields. From basic molecular biology to more applied biomedical research, IGF offers a robust and economical solution to detect fluorescent proteins in gels. Future studies could further explore the method's robustness across different cell types and conditions, ensuring its broad applicability in diverse experimental settings.

495 # Material and Methods

496 ## Yeast strains and cultures.

497 Strains are derivatives of the BY4741 background and are listed in Supplementary Table 1.
498 Proteins were tagged with various FPs at their endogenous loci by homologous recombination using
499 plasmids listed in Supplementary Table 2, or originated from the collection of GFP-tagged strains
500 (Huh et al., 2003). All yeast strains were constructed by transformation with the standard lithium
501 acetate–polyethylene glycol protocol using homologous recombination and verified by polymerase
502 chain reaction (PCR) on genomic DNA. Yeast cells were grown in YPD medium (2% w/v) or in SC
503 medium [containing yeast nitrogen base (1.7 g/L; MP Biomedicals), ammonium sulfate (5 g/liter,
504 Sigma-Aldrich), the appropriate drop-out amino acid preparations (MP Biomedicals), and 2% (w/v)
505 glucose, unless otherwise indicated]. Precultures were incubated at 30°C for 8 hours and diluted in
506 the evening to 20-mL cultures to reach mid-log phase the next morning.

507 ## Preparation of cell lysates from yeast

508 Exponentially growing cells (5 OD_{600} equivalents) were washed twice in water and resuspended
509 in 100µL of cold native lysis buffer [Tris-HCl pH 8.0, 100 mM, NaCl, 0.15 M, Glycerol 5% v/v, Triton
510 X-100 0.5% v/v, PMSF 0.5 mM, Complete antiprotease EDTA free (Roche, #11836170001)], and
511 incubated for 5 min on ice-cold water with glass beads (Sigma-Aldrich, #G8772) to cool samples
512 down prior to lysis. Cells were then lysed in a cold room on a vortex (4 x 30 sec, with 1 min incubation
513 on ice-cold water between each lysis). Cell lysates were retrieved by piercing the bottom of the 1.5-
514 mL tubes and brief centrifugation in a minispin centrifuge. Lysates were cleared by centrifugation at
515 4°C for 5 min at 3,000 xg. Supernatants were collected and 4X Laemmli sample buffer (Bio-Rad,
516 #161-0747) containing DTT (12.5 µM final concentration) was added to the lysates (1X final
517 concentration). Samples were denatured as indicated for each experiment, and loaded on a SDS-
518 PAGE gel.
519 To use IGF from colonies growing on plates for screening purposes, 3 days-old colonies were
520 harvested and resuspended in 100 µL cold native lysis buffer [Tris-HCl pH 8.0, 100 mM, NaCl, 0.15
521 M, Glycerol 5% v/v, Triton X-100 0.5% v/v, PMSF 0.5 mM, Complete antiprotease EDTA free (Roche,
522 #11836170001)] and lysed as described above for exponentially growing cells. 15 µL of lysate were
523 collected and 4X Laemmli sample buffer (Bio-Rad, #161-0747) containing DTT (12.5 µM final
524 concentration) was added to the lysates (1X final concentration). Samples were denatured at 30°C
525 for 5 min, and 20 µL were loaded on SDS-PAGE gel.
526 Relative quantitations were carried out with a detergent-compatible Bradford reagent (Abcam,
527 #ab119216), and samples were then incubated for 5 min. Denaturation temperatures varied from
528 30°C to 95°C and are indicated in the Results section and the Figures. Equivalent protein amounts

529 were loaded on commercial precast 4-20% TGX gels (Bio-Rad, #4561094), and run in Tris-glycine-
530 SDS (TGS) buffer at 150 V for 45 min unless otherwise indicated.

531 Preparation of yeast protein extracts with TCA

532 A volume of culture corresponding to 1 OD_{600} equivalent of exponentially growing yeast cells
533 was collected, to which TCA (100%, w/v; Sigma-Aldrich) was added (10% final concentration).
534 Whole cells were precipitated on ice for 10 min, samples were then centrifuged at 16,000 xg at 4°C
535 for 10 min, the pellet was resuspended in 100 µL of a 10% (w/v) TCA solution and broken for 10 min
536 with glass beads (Sigma-Aldrich, #G8772) at room temperature. Lysates were transferred to another
537 1.5-mL tube to remove glass beads and centrifuged for 5 min at 16,000 xg at 4°C. Protein pellets
538 were resuspended in 50 µL of 1X Laemmli sample buffer, which included 50 mM Tris-base (final
539 concentration) to buffer for the TCA present in the pellet.

540 Preparation of cell lysates from Drosophila cultured cells

541 Drosophila wing imaginal disc cultured cells [Clone 8 (Cl-8) cells] responsive to Hedgehog (HH)
542 were cultured and transiently transfected using transitory insect transfection reagent (Mirusbio, #
543 MIR 6100) using pAct-EGFP, pAct-SMO-EGFP, and pAct-HH (Malpel et al., 2007; Sanial et al.,
544 2017) as described previously (Sanial et al., 2017). Forty-eight hours after transfection, cells were
545 washed in PBS and lysed in 1% Triton X-100, 150 mM NaCl, 50 mM Tris-HCl pH 8.0, 1 mM
546 dithiothreitol with complete EDTA-free antiprotease mix (Roche, #11836170001) and PhosSTOP
547 (Roche, #04906837001). Lysates were centrifuged (12,000 xg) for 10 min at 4°C and the
548 supernatant was mixed with 4X Laemmli sample buffer (Bio-Rad) containing DTT (12.5 µM final
549 concentration). Samples were incubated for 5 minutes at 25°C before loading on a homemade 10%
550 acrylamide gel without SDS. Gels were run for 90 min at 150 V in TGS buffer on a MiniProtean setup
551 (Bio-Rad).

552 Preparation of cell lysates from fly ovary tissue

553 Ovary extracts were obtained from Ptub64c-GAL4 and Ptub64c-GAL4; UbiEGFP-PAR3
554 transgenic flies (Kullmann and Krahn, 2018) by dissecting ovaries (20 flies per genotype) into 1X
555 PBS. Ovaries were placed on ice in lysis buffer [10 mM Tris-HCl pH 7.5, 150 mM NaCl, Complete
556 Protease Inhibitor cocktail (Roche)] and mechanically homogenized using micro pestles in matching
557 tubes. Ovaries lysates were spun at 3000 xg for 20 min at 4°C to eliminate debris. Supernatants
558 were incubated for 5 min at 72°C in LDS sample buffer with Sample Reducing Agent (ThermoFisher,
559 #NP0007). Samples were loaded on a NuPage, 4–12% Bis-Tris gels (ThermoFisher, #NP0322) and
560 run in 1X MOPS buffer (ThermoFisher, #NP0001) for 90 min at 150v.

561 ## Preparation of cell lysates from MDCK cells

562 MDCK cells (ATCC CCL-34) were transfected with Lipofectamine 2000 (Thermofisher
563 #11668027) as described (Walch et al., 2018). Arf1-EGFP and Arf1-mCherry plasmids were
564 obtained by subcloning Arf1 (Wessels et al., 2006) into pEGFP-N3 (Clontech) and pmCherry-N1
565 (Clontech), respectively. Cells were lysed in 6-well plates at confluency with 200 µL of lysis buffer
566 [Tris-HCl pH 8.0 50 mM, NaCl 150mM, EDTA 10 mM, Triton X-100 0.5% (v/v) with complete
567 antiprotease mix (Roche #11836145001)]. After 20 min incubation on ice, cells were scraped from
568 the plate, collected in tubes and vortexed 3 x 5 sec, with 30 sec-incubation on ice between each
569 step. Lysates were cleared by centrifugation 30 min, 11000 xg at 4°C. After protein quantitation using
570 a Bradford reagent (Bio-Rad #5000205), samples were mixed with Laemmli sample buffer (Bio-Rad
571 #161-0747) (1X final concentration). 50 µg of proteins were loaded per well on a precast 4-20%TGX
572 gel (Bio-Rad, #4561094), and run in TGS buffer at 200 V for 45 min.

573 ## Preparation of cell lysates from *C. elegans*

574 Worms [*C. elegans* strain N2 (wildtype ancestral, Bristol) and JDU233: *ijmSi63 [pJD520;*
575 *mosII_5'mex-5_GFP::tba-2; mCherry::his-11; cb-unc-119(+)] II; unc-119(ed3) III* (Lacroix et al.,
576 2024)] were cultured on MGM++ plate and fed on OP50 bacterial strain at 23C. Worm lysate was
577 obtained from an asynchronous population. A total volume equivalent of 50 µL worm pellet was
578 washed twice in bacterial M9 minimal medium containing 0.05% (v/v) Tween-20, resuspended into
579 200 µL Lysis buffer [50mM Tris-HCl pH 8.0, 200 mM NaCl, 5% glycerol and Complete protease
580 inhibitor cocktail (Roche #11836145001)] and sonicated for 1 min on ice. Total extract was incubated
581 for 5 min at 50°C with 1x final pH8 Laemmli sample buffer containing DTT (12.5 µM final
582 concentration). 40 µg of worm extract were loaded per well onto a precast 4-20%TGX gel (Bio-Rad,
583 #4561094), and run in TGS buffer at 200 V for 45 min.

584 ## In-gel fluorescence imaging

585 After migration, the gel was imaged with gel-imaging systems whose excitation/emission
586 wavelengths were compatible with the observation of green and red fluorescent proteins. Imaging
587 with the Amersham Typhoon 5 (Cytiva) was carried out using the 488 nm laser with the Cy2 filter
588 525BP20 (for green FPs) or the 532 nm laser with the Cy3 filter LPG550 (for red FPs). The scanning
589 resolution was 25 µm/pixel. PMT voltage was adjusted so that collected signals do not saturate.
590 Imaging on the Chemidoc MP (Bio-Rad) was carried out using standard excitation/emission
591 wavelengths recommended for Cy2/Cy3 filters (green FP: Epi-blue, excitation: 460−490 nm,
592 emission: 518–546 nm; red FP: Epi-green, excitation: 520−545 nm, emission: 577–613 nm).
593 Total proteins were visualized by in-gel fluorescence using a trihalo compound incorporated in
594 the commercial pre-cast SDS–PAGE gels (stain-free TGX gels, 4–20%; Bio-Rad) after 45 sec UV-

595 induced photoactivation using a ChemiDoc MP imager (Bio-Rad), serving as a loading control. Note
596 that UV irradiation should preferentially be performed after FP imaging (see **Figure S2**).

597 Immunoblotting

598 After fluorescence imaging, gels were equilibrated in transfer buffer [25 mM Tris, 190 mM
599 glycine, 20% ethanol (v/v), 0.02% SDS (w/v)] for 15 min and transferred at 100 V onto a nitrocellulose
600 membrane in a liquid transfer system (MiniProtean, Bio-Rad). Membranes were blocked in Tris-
601 buffered saline solution (50 mM Tris pH 7.6, 150 mM NaCl) containing 0.1 % Tween-20 (v/v) (TBS-
602 T) and 2% fat-free milk (w/v) for 30 min and incubated for at least 2 hours with the appropriate
603 primary antibodies. Membranes were washed 3 x 10 min in TBS-T and incubated for at least two
604 hours with the corresponding secondary antibody (coupled with horseradish peroxidase or
605 Alexa680). Membranes were then washed again 3 x 10 min in TBS-T and incubated with ECL Select
606 Western Blotting Detection Reagent (Cytiva #RPN2235) except in **Figure S3B** in which Clarity
607 Western ECL Substrate (Bio-Rad #1705060) was used because of the strong signal obtained with
608 the anti-GFP antibody 3H9. Luminescence signals were acquired using a ChemiDoc MP (Bio-Rad).
609 For denaturation of proteins on the membrane (**Figure S3B**), the membrane treatment was adapted
610 from Xu et al (2019) (Xu et al., 2019): after transfer, the membrane was washed with water, incubated
611 with cold 50% methanol (v/v) on ice for 30 min. The membrane was then washed with water, quickly
612 dried on lint-free wipes and incubated in a sandwich between two sheets of Whatman paper and two
613 glass slides at 75°C in a preheated thermocycler for 30 min.

614 Antibodies

615 The primary antibodies used are: anti-GFP (clones 7.1 and 13.1; Roche #11814460001; 1/5,000
616 dilution), Anti-GFP (Chromotek #3H9; 1/5,000), anti-GFP-DyLight800 (Rockland, #600-145-215;
617 1/2,000), anti-Bmh1 (kind gift of S. Lemmon, Univ. Miami, USA; 1/15,000) (Gelperin et al., 1995);
618 anti-Hkx2 (Rockland, #100-4159; 1/3,000). Secondary antibodies are anti-Mouse IgG-HRP (Sigma-
619 Aldrich, #A5278; 1/5000), anti-Rabbit IgG-HRP (Sigma-Aldrich, #A6154; 1/5,000), anti-Rat IgG-HRP
620 (Jackson Immuno, #112-035-143; 1/5,000), and anti-Mouse IgG Alexa Fluor 680 (ThermoFisher,
621 #21057; 1/5,000).

622 Test of the linearity of the signal by sample dilution

623 Extraction was performed in native conditions using 15 OD_{600} equivalent of yeast lysed in 300
624 µL of cold native lysis buffer [100 mM Tris-HCl pH 8.0, NaCl 0.15 M, Glycerol 5% v/v, Triton X-100
625 0.5% v/v, PMSF 0.5 mM, Complete antiprotease EDTA free (Roche, #11836170001)]. 4X Laemmli
626 sample buffer (Biorad) was added to the lysates (1X final, 12.5 µM DTT final concentration), and
627 samples were then incubated for 5 min at 30°C. Samples were serial-diluted with 1X native sample
628 buffer (62.5 mM Tris-HCl pH 6.8, 10% glycerol (v/v), 0.005% bromophenol blue (w/v)], as follows: 9

629 times at 0.75X dilution, followed by 5 times at 0.5X dilution (final dilution >300 fold). Fluorescence
630 levels were quantified using ImageQuant TL v8.2 (Cytiva).

631 Sample denaturation with a range of temperatures

632 Extraction was performed in native conditions using 15OD_{600} equivalent of yeast lysed in 300µL
633 of cold native lysis buffer [100 mM Tris-HCl pH 8.0, NaCl 0.15 M, Glycerol 5% v/v, Triton X-100 0.5%
634 v/v, PMSF 0.5 mM, Complete antiprotease EDTA free (Roche, #11836170001)]. 4X Laemmli sample
635 buffer was added to the lysates (1X final, DTT 12.5 µM final concentration). Samples were distributed
636 in 0.5 mL Eppendorf tube and kept on ice until heat treatment. Samples were heated at various
637 temperatures in an Eppendorf Gradient Mastercycler for 5 min, and kept at 22°C after incubation.
638 The equivalent of 0.5 OD_{600} was loaded in each well. Fluorescence levels were quantified using
639 ImageQuant TL v8.2 (Cytiva).

640 Co-immunoprecipitations of fluorescent proteins from yeast lysates

641 Exponentially growing cells (40 OD_{600} equivalents) were washed twice in water and
642 resuspended in 400 µL of cold IP lysis buffer (100 mM Tris-HCl pH8, NaCl 200 mM, Glycerol 5%,
643 Triton X-100 0.1%, EDTA 1 mM) containing protease inhibitors [PMSF 0.5 mM, Complete
644 antiprotease EDTA free (Roche, #11836170001), NaF 10 mM], and incubated for 5 min on ice-cold
645 water with glass beads. Cells were then lysed in a cold room on a vortex (4 x 30 sec, with 1 min
646 incubation on ice-cold water between each lysis). Relative quantitation was made with Bradford
647 reagent to use equivalent amounts of proteins for co-immunoprecipitation. Samples were diluted
648 4:10 as per the manufacturer's instructions with dilution buffer (10 mM Tris-HCl pH 8.0, NaCl 200
649 mM, EDTA 1 mM) containing protease inhibitors [PMSF 0.5 mM, Complete antiprotease EDTA free
650 (Roche, #11836170001), NaF 10 mM]. A fraction (3%) was taken as the "Input" fraction. 10 µL GFP-
651 Trap Magnetic Particles M-270 (Proteintech, #gtd) or RFP-Trap Magnetic Agarose (Proteintech,
652 #rtma) were added to the remaining of the sample and incubated on a rotating wheel for 1h at 4°C
653 and washed 3 times with cold IP lysis buffer. Proteins were eluted in 40 µL of FP trap sample buffer
654 [66 mM Tris-HCl pH 8.0, 2% SDS, 100 mM NaCl, 12.5 µM DTT, 10% (v/v) glycerol, 0.002%
655 bromophenol blue (w/v)] by incubating at 50°C for 20 min with soft shaking in a dry bath incubator.
656 Half of the IP and 1% of the diluted lysate were loaded on the gel.
657

658 SNAP-tagging

659 Yeast total lysates were prepared as in "Preparation of cell lysates from yeast" using cold native
660 lysis buffer supplemented with DTT (0.5 mM final concentration). 20 µL (corresponding to 1 OD
661 equivalent) of extracts were incubated for 30 min at 37°C with 10 µL of staining solution [Tris-HCl
662 pH 8.0 100 mM, DTT 0.5 mM, PMSF 0.5 mM, Complete antiprotease EDTA free (Roche,
663 #11836170001)] in the presence or absence of SNAP-surface Alexa fluor 647 subtrate (New

664 England Biolabs, # S9136S) at a final concentration of 1.66 µM. LDS sample buffer was added (1X
665 final) and samples were denatured for 5 min at 30°C before loading onto a commercial pre-cast
666 SDS–PAGE gels (stain-free TGX gels, 4–20%; Bio-Rad).

667 Construction of yeast-optimized mCherry, mNeonGreen and FP-tagging 668 vectors

669 The mCherry and mNeonGreen sequences were codon-optimized for *Saccharomyces*
670 *cerevisiae* using GENEius tool (giving ymCherry and ymNeonGreen, respectively) and synthetized
671 (Eurofins Genomics), with a GSAGAGAGAGAG or GSGAGAGAGAGAGA linker respectively,
672 flanked by the traditional S1/S3 oligo sequences used for amplification (Janke et al., 2004). Linkers
673 were also codon-optimized but sequences are different to avoid recombination. DNA was provided
674 cloned into pEX-A128 containing a polylinker site to allow subcloning into the pYM vector series
675 (Janke et al., 2004) with various selection markers. ymNeonGreen was cloned in pYM16 at
676 BsiW1/AscI sites, giving pYM-ymCherry-NAT (pSL778), and ymCherry was cloned in pYM17 at
677 HindIII/AscI sites, giving pYM-ymNeonGreen-Hph (pSL766). Tagging with sfGFP was achieved
678 using the GTH-g plasmid (gift from Serge Pelet; Addgene #81104) (Wosika et al., 2016). Tagging
679 with mNeonGreen was achieved using pFA6-mNeongreen (HPH) plasmid (kind gift from Silke Hauf).
680 Tagging with mKO-κ was achieved using pYM GAGAGA ymKOKappa-hygro plasmid (pMC215, kind
681 gift from Aurélie Massoni). Tagging with yeast codon-optimized Tag-RFP-T or mRuby2 was
682 achieved using the pFa6-link-yoTag-RFP-T-CaURA3 and pFA6a-link-yomRuby2-SpHIS5,
683 respectively (gifts from Kurt Thorn and Wendell Lim, Addgene plasmids #44877 and #44843).
684 Tagging with EGFP was made using pYM27 (Janke et al., 2004) or by switching the GFP(S65T)-
685 HIS3MX cassette from strains originating from the GFP collection (Huh et al., 2003) to an EGFP-
686 KanMX cassette by homologous recombination. Tagging with SNAP was achieved using pBS-SKII-
687 3XHA-fSNAP-NAT (gift from Stephen Buratowski, Addgene plasmid #188916) (Baek et al., 2022).
688

689 Correlation of published protein abundance with IGF signals

690 Data of protein abundance were published in Ho et al., 2018 (Ho et al., 2018) and retrieved from
691 the Saccharomyces Genome Database (www.yeastgenome.org). For Figure 7C, average
692 abundances (±SD) were calculated for the indicated proteins using data available from non-
693 treated/unchallenged cells, and plotted against the signal intensity obtained by IGF measurement
694 normalized to total protein staining (n=3). For Figure S8, data were retrieved for abundance studies
695 based on mass spectrometry, confocal microscopy or immunoblotting and averages were calculated
696 (±SD when n≥3). Peason's correlation test was calculated for each pair (abundance and IGF signal)
697 using GraphPad Prism.

Acknowledgments

The authors wish to thank Dr Alenka Copic (CRBM, Montpellier, FR), Dr Julien Dumont (Institut Jacques Monod, Paris, FR), Dr Silke Hauf (Virginia Tech, Blacksburg, VA, USA), Dr Sandra Lemmon (University of Miami, Coral Gables, FL, USA), Mrs Aurélie Massoni (IBGC, Bordeaux, France) and Dr Myriam Ruault (Institut Curie, Paris, France) for sharing material, and Dr Catherine L. Jackson (Institut Jacques Monod, Paris, FR) for discussions and critical reading of the manuscript. This work was supported by grants from Université Paris-Cité IDEx (https://u-paris.fr; ANR-18-IDEX-0001, “Emergence en Recherche” RS30J20IDXA1_EMERLEON) and Agence Nationale pour la Recherche (“AMPKILL”, ANR-23-CE13-0012-01) to S. Léon. N. Joly is supported by a grant from the Fondation ARC pour la recherche sur le cancer (ARCPJA2022050005002) and a grant from Université Paris-Cité IDEx (https://u-paris.fr; ANR-18-IDEX-0001, “Emergence en Recherche” RS30J23IDX64_KATAREP).

The authors declare no competing interests.

711 # References

712 Aoki, T., Y. Takahashi, K.S. Koch, H.L. Leffert, and H. Watabe. 1996. Construction of a fusion protein
713 between protein A and green fluorescent protein and its application to western blotting. *FEBS*
714 *Lett*. 384:193-197.
715 Baek, I., S.N. Le, J. Jeon, Y. Chun, C. Reed, and S. Buratowski. 2022. A set of Saccharomyces
716 cerevisiae integration vectors for fluorescent dye labeling of proteins. *G3 (Bethesda)*. 12.
717 Berkelman, T.R., and J.C. Lagarias. 1986. Visualization of bilin-linked peptides and proteins in
718 polyacrylamide gels. *Anal Biochem*. 156:194-201.
719 Bird, L.E., H. Rada, A. Verma, R. Gasper, J. Birch, M. Jennions, J. Löwe, I. Moraes, and R.J. Owens.
720 2015. Green fluorescent protein-based expression screening of membrane proteins in
721 Escherichia coli. *J Vis Exp*:e52357.
722 Bomholt, J., C. Helix-Nielsen, P. Scharff-Poulsen, and P.A. Pedersen. 2013. Recombinant
723 production of human Aquaporin-1 to an exceptional high membrane density in
724 Saccharomyces cerevisiae. *PLoS One*. 8:e56431.
725 Brachmann, C.B., A. Davies, G.J. Cost, E. Caputo, J. Li, P. Hieter, and J.D. Boeke. 1998. Designer
726 deletion strains derived from Saccharomyces cerevisiae S288C: a useful set of strains and
727 plasmids for PCR-mediated gene disruption and other applications. *Yeast*. 14:115-132.
728 Butt, R.H., and J.R. Coorssen. 2013. Coomassie blue as a near-infrared fluorescent stain: a
729 systematic comparison with Sypro Ruby for in-gel protein detection. *Mol Cell Proteomics*.
730 12:3834-3850.
731 Campbell, R.E., O. Tour, A.E. Palmer, P.A. Steinbach, G.S. Baird, D.A. Zacharias, and R.Y. Tsien.
732 2002. A monomeric red fluorescent protein. *Proc Natl Acad Sci U S A*. 99:7877-7882.
733 Chalfie, M., Y. Tu, G. Euskirchen, W.W. Ward, and D.C. Prasher. 1994. Green fluorescent protein
734 as a marker for gene expression. *Science*. 263:802-805.
735 Chandris, P., C.C. Giannouli, and G. Panayotou. 2021. Imaging Approaches for the Study of
736 Metabolism in Real Time Using Genetically Encoded Reporters. *Front Cell Dev Biol*.
737 9:725114.
738 Chaudhri, M., M. Scarabel, and A. Aitken. 2003. Mammalian and yeast 14-3-3 isoforms form distinct
739 patterns of dimers in vivo. *Biochemical and Biophysical Research Communications*. 300:679-
740 685.
741 Chew, F.N., W.S. Tan, T.C. Ling, C.S. Tan, and B.T. Tey. 2009. Quantitation of green fluorescent
742 protein using a gel-based imaging method. *Anal Biochem*. 384:353-355.
743 Cormack, B.P., G. Bertram, M. Egerton, N.A.R. Gow, S. Falkow, and A.J.P. Brown. 1997. Yeast-
744 enhanced green fluorescent protein (yEGFP): a reporter of gene expression in Candida
745 albicans. *Microbiology (Reading)*. 143 (Pt 2):303-311.
746 Cormack, B.P., R.H. Valdivia, and S. Falkow. 1996. FACS-optimized mutants of the green
747 fluorescent protein (GFP). *Gene*. 173:33-38.
748 Corradi, G.R., F. de Tezanos Pinto, L.R. Mazzitelli, and H.P. Adamo. 2012. Shadows of an absent
749 partner: ATP hydrolysis and phosphoenzyme turnover of the Spf1 (sensitivity to Pichia
750 farinosa killer toxin) P5-ATPase. *J Biol Chem*. 287:30477-30484.
751 Cristea, I.M., R. Williams, B.T. Chait, and M.P. Rout. 2005. Fluorescent proteins as proteomic
752 probes. *Mol Cell Proteomics*. 4:1933-1941.
753 Donate-Macian, P., E. Alvarez-Marimon, F. Sepulcre, J.L. Vazquez-Ibar, and A. Peralvarez-Marin.
754 2019. The Membrane Proximal Domain of TRPV1 and TRPV2 Channels Mediates Protein(-
755)Protein Interactions and Lipid Binding In Vitro. *Int J Mol Sci*. 20.
756 Drew, D., M. Lerch, E. Kunji, D.J. Slotboom, and J.W. de Gier. 2006. Optimization of membrane
757 protein overexpression and purification using GFP fusions. *Nat Methods*. 3:303-313.
758 Eaton, S.L., M.L. Hurtado, K.J. Oldknow, L.C. Graham, T.W. Marchant, T.H. Gillingwater, C.
759 Farquharson, and T.M. Wishart. 2014. A guide to modern quantitative fluorescent western
760 blotting with troubleshooting strategies. *J Vis Exp*:e52099.
761 Geertsma, E.R., M. Groeneveld, D.J. Slotboom, and B. Poolman. 2008. Quality control of
762 overexpressed membrane proteins. *Proc Natl Acad Sci U S A*. 105:5722-5727.
763 Gelperin, D., J. Weigle, K. Nelson, P. Roseboom, K. Irie, K. Matsumoto, and S. Lemmon. 1995. 14-
764 3-3 proteins: potential roles in vesicular transport and Ras signaling in *Saccharomyces*
765 *cerevisiae*. *Proc Natl Acad Sci U S A*. 92:11539-11543.

766 Ho, B., A. Baryshnikova, and G.W. Brown. 2018. Unification of Protein Abundance Datasets Yields
767 a Quantitative Saccharomyces cerevisiae Proteome. *Cell Syst*. 6:192-205 e193.
768 Hochreiter, B., A.P. Garcia, and J.A. Schmid. 2015. Fluorescent proteins as genetically encoded
769 FRET biosensors in life sciences. *Sensors (Basel)*. 15:26281-26314.
770 Hovsepian, J., Q. Defenouillere, V. Albanese, L. Vachova, C. Garcia, Z. Palkova, and S. Leon. 2017.
771 Multilevel regulation of an alpha-arrestin by glucose depletion controls hexose transporter
772 endocytosis. *J Cell Biol*. 216:1811-1831.
773 Hu, C.D., and T.K. Kerppola. 2003. Simultaneous visualization of multiple protein interactions in
774 living cells using multicolor fluorescence complementation analysis. *Nat Biotechnol*. 21:539-
775 545.
776 Huh, W.K., J.V. Falvo, L.C. Gerke, A.S. Carroll, R.W. Howson, J.S. Weissman, and E.K. O'Shea.
777 2003. Global analysis of protein localization in budding yeast. *Nature*. 425:686-691.
778 Janke, C., M.M. Magiera, N. Rathfelder, C. Taxis, S. Reber, H. Maekawa, A. Moreno-Borchart, G.
779 Doenges, E. Schwob, E. Schiebel, and M. Knop. 2004. A versatile toolbox for PCR-based
780 tagging of yeast genes: new fluorescent proteins, more markers and promoter substitution
781 cassettes. *Yeast*. 21:947-962.
782 Jia, J., C. Tong, B. Wang, L. Luo, and J. Jiang. 2004. Hedgehog signalling activity of Smoothened
783 requires phosphorylation by protein kinase A and casein kinase I. *Nature*. 432:1045-1050.
784 Karasawa, S., T. Araki, T. Nagai, H. Mizuno, and A. Miyawaki. 2004. Cyan-emitting and orange-
785 emitting fluorescent proteins as a donor/acceptor pair for fluorescence resonance energy
786 transfer. *Biochem J*. 381:307-312.
787 Khmelinskii, A., P.J. Keller, A. Bartosik, M. Meurer, J.D. Barry, B.R. Mardin, A. Kaufmann, S.
788 Trautmann, M. Wachsmuth, G. Pereira, W. Huber, E. Schiebel, and M. Knop. 2012. Tandem
789 fluorescent protein timers for in vivo analysis of protein dynamics. *Nat Biotechnol*. 30:708-
790 714.
791 Koldenkova, V.P., T. Matsuda, and T. Nagai. 2015. MagIC, a genetically encoded fluorescent
792 indicator for monitoring cellular Mg2+ using a non-Forster resonance energy transfer
793 ratiometric imaging approach. *J Biomed Opt*. 20:101203.
794 Krasnoselska, G.O., M. Dumoux, N. Gamage, H. Cheruvara, J. Birch, A. Quigley, and R.J. Owens.
795 2021. Transient Transfection and Expression of Eukaryotic Membrane Proteins in Expi293F
796 Cells and Their Screening on a Small Scale: Application for Structural Studies. *Methods Mol*
797 *Biol*. 2305:105-128.
798 Kullmann, L., and M.P. Krahn. 2018. Redundant regulation of localization and protein stability of
799 DmPar3. *Cell Mol Life Sci*. 75:3269-3282.
800 Lacroix, B., S. Vigneron, J.C. Labbe, L. Pintard, C. Lionne, G. Labesse, A. Castro, and T. Lorca.
801 2024. Increases in cyclin A/Cdk activity and in PP2A-B55 inhibition by FAM122A are key
802 mitosis-inducing events. *EMBO J*. 43:993-1014.
803 Lam, A.J., F. St-Pierre, Y. Gong, J.D. Marshall, P.J. Cranfill, M.A. Baird, M.R. McKeown, J.
804 Wiedenmann, M.W. Davidson, M.J. Schnitzer, R.Y. Tsien, and M.Z. Lin. 2012. Improving
805 FRET dynamic range with bright green and red fluorescent proteins. *Nat Methods*. 9:1005-
806 1012.
807 Lambert, T.J. 2019. FPbase: a community-editable fluorescent protein database. *Nat Methods*.
808 16:277-278.
809 Laussel, C., V. Albanese, F.J. Garcia-Rodriguez, A. Ballin, Q. Defenouillere, and S. Leon. 2022. 2-
810 deoxyglucose transiently inhibits yeast AMPK signaling and triggers glucose transporter
811 endocytosis, potentiating the drug toxicity. *PLoS Genet*. 18:e1010169.
812 Lee, S., W.A. Lim, and K.S. Thorn. 2013. Improved blue, green, and red fluorescent protein tagging
813 vectors for S. cerevisiae. *PLoS One*. 8:e67902.
814 Leon, S., Z. Erpapazoglou, and R. Haguenauer-Tsapis. 2008. Ear1p and Ssh4p are new adaptors
815 of the ubiquitin ligase Rsp5p for cargo ubiquitylation and sorting at multivesicular bodies. *Mol*
816 *Biol Cell*. 19:2379-2388.
817 Longtine, M.S., A. McKenzie, 3rd, D.J. Demarini, N.G. Shah, A. Wach, A. Brachat, P. Philippsen,
818 and J.R. Pringle. 1998. Additional modules for versatile and economical PCR-based gene
819 deletion and modification in Saccharomyces cerevisiae. *Yeast*. 14:953-961.
820 Madani, G., E. Lamping, H.J. Lee, M. Niimi, A.K. Mitra, and R.D. Cannon. 2021. Small-Scale Plasma
821 Membrane Preparation for the Analysis of Candida albicans Cdr1-mGFPHis. *J Vis Exp*.

822 Malpel, S., S. Claret, M. Sanial, A. Brigui, T. Piolot, L. Daviet, S. Martin-Lanneree, and A. Plessis.
823 2007. The last 59 amino acids of Smoothened cytoplasmic tail directly bind the protein kinase
824 Fused and negatively regulate the Hedgehog pathway. *Dev Biol*. 303:121-133.
825 Merzlyak, E.M., J. Goedhart, D. Shcherbo, M.E. Bulina, A.S. Shcheglov, A.F. Fradkov, A. Gaintzeva,
826 K.A. Lukyanov, S. Lukyanov, T.W. Gadella, and D.M. Chudakov. 2007. Bright monomeric
827 red fluorescent protein with an extended fluorescence lifetime. *Nat Methods*. 4:555-557.
828 Muller-Lucks, A., S. Bock, B. Wu, and E. Beitz. 2012. Fluorescent in situ folding control for rapid
829 optimization of cell-free membrane protein synthesis. *PLoS One*. 7:e42186.
830 Nakatani, T., N. Yasui, I. Tamura, and A. Yamashita. 2019. Specific modification at the C-terminal
831 lysine residue of the green fluorescent protein variant, GFPuv, expressed in Escherichia coli.
832 *Scientific reports*. 9:4722.
833 Nemec, A.A., L.A. Howell, A.K. Peterson, M.A. Murray, and R.J. Tomko, Jr. 2017. Autophagic
834 clearance of proteasomes in yeast requires the conserved sorting nexin Snx4. *J Biol Chem*.
835 292:21466-21480.
836 Newstead, S., H. Kim, G. von Heijne, S. Iwata, and D. Drew. 2007. High-throughput fluorescent-
837 based optimization of eukaryotic membrane protein overexpression and purification in
838 Saccharomyces cerevisiae. *Proc Natl Acad Sci U S A*. 104:13936-13941.
839 Pedelacq, J.D., S. Cabantous, T. Tran, T.C. Terwilliger, and G.S. Waldo. 2006. Engineering and
840 characterization of a superfolder green fluorescent protein. *Nat Biotechnol*. 24:79-88.
841 Pincus, Z., T.C. Mazer, and F.J. Slack. 2016. Autofluorescence as a measure of senescence in C.
842 elegans: look to red, not blue or green. *Aging (Albany NY)*. 8:889-898.
843 Rodriguez, E.A., R.E. Campbell, J.Y. Lin, M.Z. Lin, A. Miyawaki, A.E. Palmer, X. Shu, J. Zhang, and
844 R.Y. Tsien. 2017. The Growing and Glowing Toolbox of Fluorescent and Photoactive
845 Proteins. *Trends Biochem Sci*. 42:111-129.
846 Romei, M.G., and S.G. Boxer. 2019. Split Green Fluorescent Proteins: Scope, Limitations, and
847 Outlook. *Annu Rev Biophys*. 48:19-44.
848 Rothbauer, U., K. Zolghadr, S. Muyldermans, A. Schepers, M.C. Cardoso, and H. Leonhardt. 2008.
849 A versatile nanotrap for biochemical and functional studies with fluorescent fusion proteins.
850 *Mol Cell Proteomics*. 7:282-289.
851 Rothbauer, U., K. Zolghadr, S. Tillib, D. Nowak, L. Schermelleh, A. Gahl, N. Backmann, K. Conrath,
852 S. Muyldermans, M.C. Cardoso, and H. Leonhardt. 2006. Targeting and tracing antigens in
853 live cells with fluorescent nanobodies. *Nat Methods*. 3:887-889.
854 Ruan, Z., J. Lee, Y. Li, J. Du, and W. Lu. 2024. Human pannexin 1 channel is not phosphorylated
855 by Src tyrosine kinase at Tyr199 and Tyr309. *eLife*. 13:eLife.95118.
856 Saeed, I.A., and S.S. Ashraf. 2009. Denaturation studies reveal significant differences between GFP
857 and blue fluorescent protein. *Int J Biol Macromol*. 45:236-241.
858 Sanial, M., I. Becam, L. Hofmann, J. Behague, C. Arguelles, V. Gourhand, L. Bruzzone, R.A.
859 Holmgren, and A. Plessis. 2017. Dose-dependent transduction of Hedgehog relies on
860 phosphorylation-based feedback between the G-protein-coupled receptor Smoothened and
861 the kinase Fused. *Development*. 144:1841-1850.
862 Shaner, N.C., R.E. Campbell, P.A. Steinbach, B.N. Giepmans, A.E. Palmer, and R.Y. Tsien. 2004.
863 Improved monomeric red, orange and yellow fluorescent proteins derived from Discosoma
864 sp. red fluorescent protein. *Nat Biotechnol*. 22:1567-1572.
865 Shaner, N.C., G.G. Lambert, A. Chammas, Y. Ni, P.J. Cranfill, M.A. Baird, B.R. Sell, J.R. Allen, R.N.
866 Day, M. Israelsson, M.W. Davidson, and J. Wang. 2013. A bright monomeric green
867 fluorescent protein derived from Branchiostoma lanceolatum. *Nat Methods*. 10:407-409.
868 Shaner, N.C., M.Z. Lin, M.R. McKeown, P.A. Steinbach, K.L. Hazelwood, M.W. Davidson, and R.Y.
869 Tsien. 2008. Improving the photostability of bright monomeric orange and red fluorescent
870 proteins. *Nat Methods*. 5:545-551.
871 Shaner, N.C., P.A. Steinbach, and R.Y. Tsien. 2005. A guide to choosing fluorescent proteins. *Nat*
872 *Methods*. 2:905-909.
873 Shcherbakova, D.M., M. Baloban, and V.V. Verkhusha. 2015. Near-infrared fluorescent proteins
874 engineered from bacterial phytochromes. *Curr Opin Chem Biol*. 27:52-63.
875 Stepanenko, O.V., I.M. Kuznetsova, K.K. Turoverov, and O.V. Stepanenko. 2022. Impact of Double
876 Covalent Binding of BV in NIR FPs on Their Spectral and Physicochemical Properties. *Int J*
877 *Mol Sci*. 23.

878 Subach, F.V., O.M. Subach, I.S. Gundorov, K.S. Morozova, K.D. Piatkevich, A.M. Cuervo, and V.V.
879 Verkhusha. 2009. Monomeric fluorescent timers that change color from blue to red report on
880 cellular trafficking. *Nat Chem Biol*. 5:118-126.
881 Terskikh, A., A. Fradkov, G. Ermakova, A. Zaraisky, P. Tan, A.V. Kajava, X. Zhao, S. Lukyanov, M.
882 Matz, S. Kim, I. Weissman, and P. Siebert. 2000. "Fluorescent timer": protein that changes
883 color with time. *Science*. 290:1585-1588.
884 Tirat, A., F. Freuler, T. Stettler, L.M. Mayr, and L. Leder. 2006. Evaluation of two novel tag-based
885 labelling technologies for site-specific modification of proteins. *Int J Biol Macromol*. 39:66-76.
886 Tsien, R.Y. 1998. The green fluorescent protein. *Annu Rev Biochem*. 67:509-544.
887 Tsutsui, H., S. Karasawa, Y. Okamura, and A. Miyawaki. 2008. Improving membrane voltage
888 measurements using FRET with new fluorescent proteins. *Nat Methods*. 5:683-685.
889 Wach, A., A. Brachat, C. Alberti-Segui, C. Rebischung, and P. Philippsen. 1997. Heterologous HIS3
890 marker and GFP reporter modules for PCR-targeting in Saccharomyces cerevisiae. *Yeast*.
891 13:1065-1075.
892 Walch, L., E. Pellier, W. Leng, G. Lakisic, A. Gautreau, V. Contremoulins, J.M. Verbavatz, and C.L.
893 Jackson. 2018. GBF1 and Arf1 interact with Miro and regulate mitochondrial positioning
894 within cells. *Scientific reports*. 8:17121.
895 Wang, M., Y. Da, and Y. Tian. 2023. Fluorescent proteins and genetically encoded biosensors.
896 *Chem Soc Rev*. 52:1189-1214.
897 Ward, W.W. 2005. Biochemical and Physical Properties of Green Fluorescent Protein. *In* Green
898 Fluorescent Protein. 39-65.
899 Weinberger Ii, J., and C.W. Lennon. 2021. Monitoring Protein Splicing Using In-gel Fluorescence
900 Immediately Following SDS-PAGE. *Bio Protoc*. 11:e4121.
901 Wessels, E., D. Duijsings, T.K. Niu, S. Neumann, V.M. Oorschot, F. de Lange, K.H. Lanke, J.
902 Klumperman, A. Henke, C.L. Jackson, W.J. Melchers, and F.J. van Kuppeveld. 2006. A viral
903 protein that blocks Arf1-mediated COP-I assembly by inhibiting the guanine nucleotide
904 exchange factor GBF1. *Dev Cell*. 11:191-201.
905 White, J., and E. Stelzer. 1999. Photobleaching GFP reveals protein dynamics inside live cells.
906 *Trends Cell Biol*. 9:61-65.
907 Wosika, V., E. Durandau, C. Varidel, D. Aymoz, M. Schmitt, and S. Pelet. 2016. New families of
908 single integration vectors and gene tagging plasmids for genetic manipulations in budding
909 yeast. *Mol Genet Genomics*. 291:2231-2240.
910 Xu, J., H. Sun, G. Huang, G. Liu, Z. Li, H. Yang, L. Jin, X. Cui, L. Shi, T. Ma, A. Kameyama, and W.
911 Dong. 2019. A fixation method for the optimisation of western blotting. *Scientific reports*.
912 9:6649.
913 Xu, Q., and T.A. Keiderling. 2004. Effect of sodium dodecyl sulfate on folding and thermal stability
914 of acid-denatured cytochrome c: a spectroscopic approach. *Protein Sci*. 13:2949-2959.
915 Yanushevich, Y.G., D.B. Staroverov, A.P. Savitsky, A.F. Fradkov, N.G. Gurskaya, M.E. Bulina, K.A.
916 Lukyanov, and S.A. Lukyanov. 2002. A strategy for the generation of non-aggregating
917 mutants of Anthozoa fluorescent proteins. *FEBS Lett*. 511:11-14.
918 Zacharias, D.A., J.D. Violin, A.C. Newton, and R.Y. Tsien. 2002. Partitioning of lipid-modified
919 monomeric GFPs into membrane microdomains of live cells. *Science*. 296:913-916.
920

921

922 # Figure legends

923 Figure 1. Detection of in-gel fluorescence from endogenously expressed proteins
924 tagged with yeGFP.

925 A. Control (WT) yeast or yeast expressing Bmh1-yeGFP, Hxk1-yeGFP were lysed in the
926 indicated conditions (Nat.: native conditions; TCA: lysis in denaturing conditions with TCA),
927 samples were resuspended in LDS sample buffer (1X final, Bio-Rad) and incubated for 5 min
928 at the indicated temperatures. After migration on a commercial precast 4-20% TGX gels (Bio-
929 Rad), gels were imaged for green fluorescence using a Typhoon and a Chemidoc MP, and
930 total proteins were visualized by the stain-free technology on a Chemidoc MP. After transfer
931 to a nitrocellulose membrane, proteins were immunoblotted with anti-GFP antibodies
932 (Roche) and detected by chemiluminescence using anti-mouse antibodies coupled to HRP.
933 B. Protein lysates were prepared as in A. Proteins were incubated at 30°C or 95°C for 5 min,
934 with and without prior incubation at 30°C (5 min). After migration on a commercial precast 4-
935 20%TGX gel (Bio-Rad), gels were imaged for green fluorescence using a Chemidoc MP, and
936 total proteins were visualized by the stain-free technology on a Chemidoc MP. Proteins were
937 then transferred to a nitrocellulose membrane and imaged again for yeGFP fluorescence,
938 which was maintained during transfer. Proteins were then immunoblotted with anti-GFP
939 antibodies (Roche) and anti-mouse antibodies coupled to Alexa Fluor 680. yeGFP
940 fluorescence was then visualized again before detecting the anti-GFP antibodies by
941 fluorescence on a Chemidoc MP.

942 Figure 2. Comparison of in-gel fluorescence of yeGFP-, GFP(S65T)- and EGFP-tagged
943 proteins

944 A. Yeast expressing Bmh1-yeGFP, Bmh1-GFP(S65T), Hxk1-yeGFP and Hxk1-GFP(S65T)
945 were lysed in native conditions, samples were resuspended in LDS sample buffer and
946 incubated for 5 min at the indicated temperatures. After migration on a commercial precast
947 4-20% TGX gels (Bio-Rad), gels were imaged for green fluorescence using a Chemidoc MP,
948 and total proteins were visualized by the stain-free technology on a Chemidoc MP. Proteins
949 were then transferred to a nitrocellulose membrane and imaged again for green
950 fluorescence, which was maintained during transfer. Proteins were then immunoblotted with
951 anti-GFP antibodies (Roche) and anti-mouse antibodies coupled to Alexa Fluor 680. Green
952 fluorescence was then visualized again before detecting the anti-GFP antibodies by
953 fluorescence. The membranes were then stripped and incubated with anti-Bmh1 or anti-
954 Hxk1/2 antibodies and then with anti-rabbit antibodies coupled to HRP, and revealed by
955 chemiluminescence on a Chemidoc MP.

956 B. Yeast expressing Bmh1-yeGFP and Bmh1-EGFP were lysed in native conditions, samples
957 were resuspended in LDS sample buffer and incubated for 5 min at the indicated
958 temperatures. After migration on a commercial precast 4-20% TGX gel (Bio-Rad), gels were
959 imaged for green fluorescence using a Typhoon or a Chemidoc MP, and total proteins were
960 visualized by the stain-free technology on a Chemidoc MP. Proteins were then transferred to
961 a nitrocellulose membrane and immunoblotted with anti-Bmh1 antibodies and then with anti-
962 rabbit antibodies coupled to HRP, and revealed by chemiluminescence on a Chemidoc MP.
963 * indicates the fluorescent species.

964 Figure 3. Comparison of in-gel fluorescence of yeGFP-, sfGFP- and mNeonGreen-
965 tagged proteins

966 Yeast expressing Bmh1-yeGFP, Bmh1-sfGFP or Bmh1-mNeonGreen were lysed in native
967 conditions, samples were resuspended in LDS sample buffer and incubated for 5 min at the
968 indicated temperatures. After migration on a commercial precast 4-20%TGX gel (Bio-Rad), gels
969 were imaged for green fluorescence using a Typhoon or a Chemidoc MP, and total proteins were
970 visualized by the stain-free technology on a Chemidoc MP. Proteins were then transferred to a
971 nitrocellulose membrane and immunoblotted with anti-Bmh1 antibodies and then with anti-rabbit
972 antibodies coupled to HRP, and revealed by chemiluminescence on a Chemidoc MP. * indicates
973 the fluorescent species.

974 Figure 4. Temperature-sensitivity of in-gel fluorescence of yeGFP-, EGFP- and sfGFP-
975 tagged proteins

976 A. Yeast expressing Bmh1-yeGFP were lysed in native conditions, samples were resuspended
977 in LDS sample buffer and incubated for 5 min at the indicated temperatures in a gradient
978 thermocycler (note that the temperature range is different for sfGFP). After migration on a
979 commercial precast 4-20%TGX gel (Bio-Rad), gels were imaged for green fluorescence
980 using a Typhoon, and total proteins were visualized by the stain-free technology on a
981 Chemidoc MP. Proteins were then transferred to a nitrocellulose membrane and
982 immunoblotted with anti-Bmh1 antibodies and then with anti-rabbit antibodies coupled to
983 HRP, and revealed by chemiluminescence on a Chemidoc MP.
984 B. Same as A. using yeast expressing Bmh1-EGFP.
985 C. Same as A. using yeast expressing Bmh1-sfGFP.
986 D. Quantification of the green fluorescence signal as a function of the denaturation temperature
987 for various green FP-tagged Bmh1 (n=3; ± SD). Solid line: sigmoidal fit of the data (GraphPad
988 Prism), dotted line: 95% confidence interval of the fit.

989 Figure 5. Comparison of in-gel fluorescence of tagRFP-T-, mRuby2-, mCherry- and
990 mKO-κ-tagged proteins

991 A. Yeast expressing Bmh1-tagRFP-T, Bmh1-mRuby2, Bmh1-mCherry or Bmh1-mKO-κ were
992 lysed in native conditions, samples were resuspended in LDS sample buffer and incubated
993 for 5 min at the indicated temperatures. After migration on a commercial precast 4-20%TGX
994 gel (Bio-Rad), gels were imaged for red fluorescence using a Typhoon or a Chemidoc MP,
995 and total proteins were visualized by the stain-free technology on a Chemidoc MP. Proteins
996 were then transferred to a nitrocellulose membrane and immunoblotted with anti-Bmh1
997 antibodies and then with anti-rabbit antibodies coupled to HRP, and revealed by
998 chemiluminescence on a Chemidoc MP. * indicates the fluorescent species.
999 B. Yeast expressing Bmh1-mCherry were lysed in native conditions, samples were
1000 resuspended in LDS sample buffer and incubated for 5 min at the indicated temperatures in
1001 a gradient thermocycler. After migration on a commercial precast 4-20%TGX gel (Bio-Rad),
1002 gels were imaged for red fluorescence using a Typhoon, and total proteins were visualized
1003 by the stain-free technology on a Chemidoc. Proteins were then transferred to a nitrocellulose
1004 membrane and immunoblotted with anti-Bmh1 antibodies and then with anti-rabbit antibodies
1005 coupled to HRP, and revealed by chemiluminescence on a Chemidoc MP.
1006 C. Same as (B) on lysates of yeast expressing Bmh1-mKO-κ.
1007 D. Quantification of the fluorescence signal as a function of the denaturation temperature for
1008 mCherry-tagged and mKO-κ-tagged Bmh1 (n=3; ±SD). Solid line: sigmoidal fit of the data
1009 (GraphPad Prism), dotted line: 95% confidence interval of the fit.

1010 Figure 6. Sensitivity and linearity of in-gel fluorescence detection of EGFP

1011 A. *Left.* Yeast expressing Bmh1-EGFP were lysed in native conditions, samples were
1012 resuspended in LDS sample buffer and incubated for 5 min at 30°C. Samples were serially
1013 diluted (right to left) into sample buffer without LDS (see Material and Methods), and loaded
1014 onto on a commercial precast 4-20%TGX gel (Bio-Rad). After migration, gels were imaged
1015 for green fluorescence using a Typhoon, and proteins were then transferred to a
1016 nitrocellulose membrane and immunoblotted with anti-Bmh1 antibodies and then with anti-
1017 rabbit antibodies coupled to HRP, and revealed by chemiluminescence on a Chemidoc MP.
1018 *Right.* Quantification of the signals obtained for green fluorescence (black) and
1019 chemiluminescence (red) as a function of sample dilution. Linear-scaled and log-plot scaled
1020 graphs are shown. The regression coefficient of a linear fitting is indicated.
1021 B. *Left.* Same experiment as in A, but using anti-GFP antibodies and anti-mouse antibodies
1022 coupled to HRP to reveal proteins by chemiluminescence. *Right.* Quantification of the signals
1023 obtained for fluorescence (black) and chemiluminescence (red) as a function of sample

1024 dilution. Linear-scaled and log-plot scaled graphs are shown. The regression coefficient of a
1025 linear fitting is indicated.

1026 Figure 7. Detection of endogenous yeast EGFP-tagged proteins with various expression
1027 levels and correlation with published abundances.

1028 A. Proteins tagged with EGFP for IGF detection. Abundance (median) is according to Ho et al.,
1029 2018 (Ho et al., 2018) and available at www.yeastgenome.org. PM: plasma membrane, ER:
1030 endoplasmic reticulum.
1031 B. Protein lysates prepared in native conditions from yeast expressing the indicated proteins
1032 fused to EGFP. Samples were resuspended in LDS sample buffer and incubated for 5 min
1033 at the 30°C and loaded onto on a commercial precast 4-20%TGX gel (Bio-Rad). After
1034 migration, gels were imaged for green fluorescence using a Typhoon, and total proteins
1035 were visualized by the stain-free technology on a Chemidoc MP. A representative gel is
1036 shown.
1037 C.

1038 Figure 8. IGF detection in the context of co-immunoprecipitation or SNAP-tagging

1039 A. Protein lysates prepared in native conditions with native IP lysis buffer from yeast expressing
1040 Bmh2-ymCherry (a yeast codon-optimized mCherry) with or without the co-expression of
1041 Bmh1-yeGFP were subjected to co-immunoprecipitation using GFP-trap beads.
1042 Immunoprecipitates were incubated at 50°C for 20 min in 1X Laemmli sample buffer at pH
1043 8.0 which allows to maintain protein fluorescence at low protein concentrations. Input
1044 samples and immunoprecipitates (IP) are shown. After migration on a commercial precast 4-
1045 20%TGX gel (Bio-Rad), gels were imaged for green and red fluorescence using a Typhoon,
1046 and total proteins were visualized by the stain-free technology on a Chemidoc MP. * indicates
1047 bleed-through of the green fluorescence into the red channel.
1048 B. Protein lysates prepared in native conditions from yeast expressing Bmh1-yeGFP with or
1049 without the co-expression of Bmh2-ymCh were subjected to co-immunoprecipitation using
1050 RFP-trap beads and treated as in A. Input samples and immunoprecipitates (IP) are shown.
1051 After migration on a commercial precast 4-20%TGX gel (Bio-Rad), gels were imaged for
1052 green and red fluorescence using a Typhoon, and total proteins were visualized by the stain-
1053 free technology on a Chemidoc MP.
1054 C. Protein lysates prepared in native conditions with native IP lysis buffer from yeast expressing
1055 Reg1-SNAP and Snf4-mCherry, and were treated or not with SNAP-surface Alexa Fluor 647.
1056 After migration on a commercial precast 4-20%TGX gel (Bio-Rad), gels were imaged for red
1057 and far-red fluorescence using a Typhoon, and total proteins were visualized by the stain-
1058 free technology on a Chemidoc MP.

1059 Figure 9. IGF detection in cells from various organisms

1060 A. Drosophila wing-imaginal-disc cultured cells [Clone 8 (Cl-8) cells] were transfected with
1061 plasmids encoding the Hedgehog (HH) transducer Smoothened (SMO) fused to EGFP and
1062 EGFP alone. They were also transfected (+) or not (-) with a construct allowing the
1063 expression of HH. Cells were lysed in native conditions (see Material and Methods), lysates
1064 were mixed with 4X Laemmli sample buffer and incubated for 5 minutes at 25°C before
1065 loading on a homemade PAGE gel. IGF was detected on a Typhoon. SMO-EGFP is
1066 phosphorylated in the presence of HH, causing a slower migration (red arrowhead).
1067 B. Transgenic *Drosophila* flies expressing or not an EGFP-tagged version of the polarity protein
1068 PAR-3 were dissected and ovaries were lysed in native conditions (see Material and
1069 Methods). Samples were incubated for 5 min at 72°C in LDS sample buffer, loaded on a
1070 NuPage Bis-Tris gel (ThermoFisher) and IGF was detected on a Typhoon after migration.
1071 After fluorescence imaging, total proteins were stained with Coomassie stain and imaged on
1072 the infrared channel on a Chemidoc MP.
1073 C. MDCK cells expressing Arf1 fused to EGFP or mCherry were lysed in native conditions (see
1074 Material and Methods). Samples were incubated for 10 min at 50°C in LDS sample buffer
1075 and loaded on a gel. After migration on a commercial precast 4-20%TGX gel (Bio-Rad), gels
1076 were imaged for green and red fluorescence using a Chemidoc MP, and total proteins were
1077 visualized by the stain-free technology on a Chemidoc MP. Note that some bleed-through of
1078 green fluorescence is observed in the red channel (see also **Figure 8A** and **Figure S9**).
1079 D. Transgenic *C. elegans* expressing or not GFP-tagged alpha-tubulin and mCherry-tagged
1080 histone H2B were lysed in native conditions (see Material and Methods) by sonication.
1081 Samples were incubated for 5 min at 30°C or 50°C in Laemmli sample buffer (pH 8.0). After
1082 migration on a commercial precast 4-20%TGX gel (Bio-Rad), gels were imaged for green
1083 and red fluorescence using a Typhoon, and total proteins were visualized by the stain-free
1084 technology on a Chemidoc MP. * denotes a non-specific fluorescence protein present in
1085 extracts of WT *C. elegans* whose fluorescence disappears when heating the sample at 50°C.

1086 Figure 10. Overview of the workflow and technical considerations when using IGF
1087 detection to visualize proteins in gel.

1088 Overview of the IGF protocol. Lysis should be made in non-denaturing conditions to preserve
1089 endogenous fluorescence. Reagents tested include TX-100 (1%, **Figure 9A**), EDTA (10 mM, **Figure**
1090 **9C**), DTT (2 mM, **Figure 9C**), antiprotease and antiphosphatase cocktails (**Figure 9C**), PMSF (0.5
1091 mM), NaF (10 mM, **Figure 8**). Samples can be resuspended in classical Laemmli buffer containing
1092 SDS or LDS (12.5 µM DTT). Denaturation can be done preferentially for 5 min at 30°C, although
1093 longer times and higher temperatures were also tested throughout the study (**Figures 3, 4, 5**). For
1094 co-immunoprecipitation experiments, care should be taken to use a specific buffer to resuspend

1095 immunoprecipitates (Tris-HCl 66 mM pH 8.0, SDS 2%, NaCl 0.1 M, DTT 12.5 µM) to avoid
1096 denaturation occurring in diluted samples (**Figure S6B**). Samples can be frozen if needed (-20°C, -
1097 80°C, liquid nitrogen, **Figure S2A**). Migration was generally done in TGX gels in regular TGS buffer,
1098 although NuPAGE Bis-Tris Gels were also used in MOPS buffer (**Figure 9B**). Migration at lower
1099 voltage than usual prevents overheating and FP denaturation. For faster migrations, the
1100 electrophoresis tank can be placed in ice-cold water, or pre-chilled buffer can be used. Note that
1101 Prestained protein ladders are fluorescent (**Figure S10**). Use unstained ladder or load a few
1102 microliters of prestained ladder. After uncasting, cut blue migration front to avoid fluorescence signal.
1103 Keep gel in water (no transfer buffer) and handle with clean gloves to avoid stains. Fluorescence
1104 imaging should be preferentially done before visualizing total proteins with UVs ("Stain-free") (**Figure**
1105 **S2B**). Note that green fluorescence may bleed through in the red channel (**Figures 8A, S9**). Total
1106 protein staining can also be performed by Coomassie staining, which can be quantified in the near-
1107 infrared (**Figure S9B**) or with silver nitrate. Transfer can also be performed after fluorescence
1108 imaging, with maintenance of the FP fluorescence on the membrane (**Figure 1**) if no Ponceau
1109 staining was applied, and before addition of the chemiluminescent reagent as fluorescence is not
1110 maintained in hydrogen peroxide solution. Protein denaturation on membrane can increase antibody
1111 detection of low temperature-treated samples (**Figure S3B**).
1112
1113

1114 # Supplementary material

1115 ## Supplementary tables.

1116 **Table S1: Yeast strains used in this study**

Name	Genotype & Description	Origin & Reference
ySL0066: **BY4741 (WT)**	*MAT a; ura3Δ0, his3Δ1, leu2Δ0, met15Δ0*	(Brachmann et al., 1998)
ySL2719: **Bmh1-yeGFP**	*MAT a; ura3Δ0, his3Δ1, leu2Δ0, met15Δ0; BMH1-yeGFP::KANMX*	This study
ySL3509: **Hxk1-yeGFP**	*MAT a; ura3Δ0, his3Δ1, leu2Δ0, met15Δ0; HXK1-yeGFP::HPHNT1*	This study
ySL0435: **Bmh1-GFP(S65T)**	*MAT a; ura3Δ0, his3Δ1, leu2Δ0, met15Δ0; BMH1:GFP(S65T)::HIS3MX6*	(Huh et al., 2003)
ySL3674: **Bmh1-EGFP**	*MAT a; ura3Δ0, his3Δ1, leu2Δ0, met15Δ0; BMH1-EGFP::HIS3MX6*	This study
ySL3419: **Bmh1-mCherry**	*MAT a; ura3Δ0, his3Δ1, leu2Δ0, met15Δ0; BMH1-mCherry::KANMX4*	This study
ySL3420: **Bmh1-mRuby2**	*MAT a; ura3Δ0, his3Δ1, leu2Δ0, met15Δ0; BMH1-mRUBY2::HIS3MX6*	This study
ySL3421: **Bmh1-TagRFP-T**	*MAT a; ura3Δ0, his3Δ1, leu2Δ0, met15Δ0; BMH1-TagRFP-T::CaURA3*	This study
ySL3422: **Bmh1-sfGFP**	*MAT a; ura3Δ0, his3Δ1, leu2Δ0, met15Δ0; BMH1-sfGFP::HIS3MX6*	This study
ySL3423: **Bmh1-mNeongreen**	*MAT a; ura3Δ0, his3Δ1, leu2Δ0, met15Δ0; BMH1-mNeonGreen::HPHNT1*	This study
ySL3512: **Reg1-3HA-SNAP**	*Mat a ; his3Δ1 leu2Δ0 met15Δ0 ura3Δ0; REG1-3xHA-SNAP::NAT*	This study
ySL3591: **Bmh1-ymNeongreen**	*MAT a; ura3Δ0, his3Δ1, leu2Δ0, met15Δ0; BMH1-ymNeonGreen::HPHNT1*	This study
ySL3593: **Bmh2-ymCherry**	*MAT a; ura3Δ0, his3Δ1, leu2Δ0, met15Δ0; BMH2-ymCherry::NATNT2*	This study
ySL3595: **Bmh2-ymCherry Bmh1-yeGFP**	*MAT a; ura3Δ0, his3Δ1, leu2Δ0, met15Δ0; BMH1-GFP::KanMx4; BMH2-ymCherry::NATNT2*	This study
ySL3684: **Reg1-EGFP**	*MAT a; ura3Δ0, his3Δ1, leu2Δ0, met15Δ0; REG1-EGFP::KanMx4*	This study
ySL3770: **Bmh1-ymKO-κ**	*MAT a; ura3Δ0, his3Δ1, leu2Δ0, met15Δ0; BMH1-ymKOκ::HPHNT1*	This study
ySL4016: **Kip3-EGFP**	*Mat a ; his3Δ1 leu2Δ0 met15Δ0 ura3Δ0 KIP3-EGFP::kanMX*	This study
ySL4017: **Hxt5-EGFP**	*Mat a ; his3Δ1 leu2Δ0 met15Δ0 ura3Δ0 HXT5-EGFP::kanMX*	This study
ySL4018: **Fkh1-EGFP**	*Mat a ; his3Δ1 leu2Δ0 met15Δ0 ura3Δ0 FKH1-EGFP::kanMX*	This study
ySL4019: **Rod1-EGFP**	*Mat a ; his3Δ1 leu2Δ0 met15Δ0 ura3Δ0 ROD1-EGFP::kanMX*	This study
ySL4020: **Apl1-EGFP**	*Mat a ; his3Δ1 leu2Δ0 met15Δ0 ura3Δ0 APL1-EGFP::kanMX*	This study
ySL4021: **mRpl25-EGFP**	*Mat a ; his3Δ1 leu2Δ0 met15Δ0 ura3Δ0 MRPL25-EGFP::kanMX*	This study
ySL4022: **Rtk1-EGFP**	*Mat a ; his3Δ1 leu2Δ0 met15Δ0 ura3Δ0 RTK1-EGFP::kanMX*	This study
ySL4023: **Sdh2-EGFP**	*Mat a ; his3Δ1 leu2Δ0 met15Δ0 ura3Δ0 SDH2-EGFP::kanMX*	This study
ySL4024: **Snf1-EGFP**	*Mat a ; his3Δ1 leu2Δ0 met15Δ0 ura3Δ0 SNF1-EGFP::kanMX*	This study
ySL4025: **Ina1-EGFP**	*Mat a ; his3Δ1 leu2Δ0 met15Δ0 ura3Δ0 INA1-EGFP::kanMX*	This study
ySL4026: **Rpa12-EGFP**	*Mat a ; his3Δ1 leu2Δ0 met15Δ0 ura3Δ0 RPA12-EGFP::kanMX*	This study
ySL4027: **Ade16-EGFP**	*Mat a ; his3Δ1 leu2Δ0 met15Δ0 ura3Δ0 ADE16-EGFP::kanMX*	This study
ySL4028: **Spf1-EGFP**	*Mat a ; his3Δ1 leu2Δ0 met15Δ0 ura3Δ0 SPF1-EGFP::kanMX*	This study
ySL4029: **Pre6-EGFP**	*Mat a ; his3Δ1 leu2Δ0 met15Δ0 ura3Δ0 PRE6-EGFP::kanMX*	This study
ySL4030: **Ipp1-EGFP**	*Mat a ; his3Δ1 leu2Δ0 met15Δ0 ura3Δ0 IPP1-EGFP::kanMX*	This study

1117

1118

1119 **Table S2: Plasmids for yeast tagging used in this study**

1120

Name	Description	Origin & Reference
pYM12	Plasmid to tag genes with yeGFP at their endogenous locus (*KANMX4*)	(Janke et al., 2004)
pYM25	Plasmid to tag genes with EGFP at their endogenous locus (*HPHNT1*)	(Janke et al., 2004)
pYM28	Plasmid to tag genes with EGFP at their endogenous locus (*HIS3MX6*)	(Janke et al., 2004)
GTH-g (pSL648)	Plasmid to tag genes with sfGFP at their endogenous locus (*HIS3MX6*)	Addgene #81104 (Wosika et al., 2016)
pFA6-mNeongreen::Hph (pSL643)	Plasmid to tag genes with mNeonGreen at their endogenous locus (*HPHNT1*)	Silke Hauf's lab, Virginia Tech; unpublished
pFa6-link-yoTag-RFP-T-CaURA3 (pSL558)	Plasmid to tag genes with yeast codon-optimized Tag-RFP-T at their endogenous locus (*CaURA3*)	Addgene #44877 (Lee et al., 2013)
pFA6a-link-yomRuby2-SpHIS5 (pS649)	Plasmid to tag genes with yeast codon-optimized mRuby2 at their endogenous locus (*SpHIS5*)	Addgene #44843 (Lee et al., 2013)
pYM-mCherry (pSL1)	Plasmid to tag genes with mCherry at their endogenous locus (*KANMX4*)	(Leon et al., 2008)
pYM-ymCherry-NAT (pSL778)	Plasmid to tag genes with yeast codon-optimized mCherry (*NATNT2*)	This study
pYM-ymNeonGreen-Hph (pSL766)	Plasmid to tag genes with yeast codon-optimized mNeonGreen (*HPHNT1*)	This study
pYM ymKO-κ-Hph (pMC215)	Plasmid to tag genes with yeast codon-optimized mKO-κ (*HPHNT1*)	Aurélie Massoni, IBGC, France; unpublished

1121

1122

1123 # Supplementary Figure legends.

1124 Supplementary Figure 1. Spectral properties of green fluorescent proteins used in this
1125 study.

1126 A. Excitation wavelengths of yeGFP (= GFPmut3), EGFP, sfGFP and mNeonGreen. Data were
1127 retrieved from FPBase (Lambert, 2019). The window of excitation provided by the Chemidoc
1128 MP imaging system is indicated in gray (460-490nm), the wavelength of the excitation laser
1129 of the Typhoon is indicated as a dotted line (488 nm), as per the manufacturer's indications.
1130 B. Emission wavelengths of yeGFP (=GFPmut3), EGFP, sfGFP, and mNeonGreen. Data were
1131 retrieved from FPBase (Lambert, 2019). The window of emission collected by the Chemidoc
1132 MP system is indicated in gray (518-546 nm), that of the Typhoon is indicated as shaded
1133 (515-535 nm), as per the manufacturer's indications.

1134 Supplementary Figure 2. Effect of UV irradiation and freezing on the fluorescence of
1135 various fluorescent proteins.

1136 A. Native lysates of cells expressing Bmh1 tagged with yeGFP, EGFP, sfGFP, mNeonGreen,
1137 mCherry or mKO-κ were kept on ice or frozen (-20°C, -80°C, or in liquid N_2) for one hour,
1138 thawed on ice and incubated at 30°C for 5 min, and loaded onto SDS-PAGE. IGF was
1139 detected on a Chemidoc MP before (top) and after (bottom) UV irradiation, which is required
1140 for the "StainFree" labeling (Bio-Rad) of total proteins with a trihalo compound (see Material
1141 and Methods).
1142 B. Quantification of the effect of UV exposure on IGF (ratio of signal obtained after UV exposure
1143 to that obtained before UV exposure, for each fluorophore; n=4; ± SD).

1144 Supplementary Figure 3. Effect of denaturation temperature on the recognition of GFP-
1145 tagged proteins by various anti-GFP antibodies.

1146 A. A native lysate of cells expressing Bmh1-yeGFP was resuspended in LDS sample buffer and
1147 incubated at the indicated temperatures. After migration, gels were imaged for green
1148 fluorescence using a Chemidoc MP, and total proteins were visualized by the stain-free
1149 technology on a Chemidoc MP. Proteins were then transferred to a nitrocellulose membrane,
1150 immunoblotted with the indicated antibodies and revealed using fluorescent secondary
1151 antibodies on a Chemidoc MP. * indicates the fluorescent species.
1152 B. A native lysate of cells expressing Bmh1-yeGFP was resuspended in LDS sample buffer and
1153 incubated at the indicated temperatures. After migration, gels were imaged for green
1154 fluorescence using a Chemidoc MP, and total proteins were visualized by the stain-free
1155 technology on a Chemidoc MP. Proteins were then transferred to a nitrocellulose membrane
1156 and immunoblotted with the indicated antibodies and revealed by chemiluminescence on a

1157 Chemidoc MP. Membranes on the right were treated with methanol and high temperature
1158 (see Material and Methods) to denature proteins and ameliorate the detection of GFP-tagged
1159 proteins treated at low temperatures. * indicates the fluorescent species.

1160 Supplementary Figure 4. Comparison of IGF signals of mNeonGreen and a
1161 corresponding yeast-optimized version.

1162 Yeast expressing Bmh1-mNG and Bmh1-ymNG were lysed in native conditions, samples
1163 were resuspended in LDS sample buffer and incubated for 5 min at the indicated temperatures. After
1164 migration, gels were imaged for green fluorescence using a Typhoon or a Chemidoc MP, and total
1165 proteins were visualized by the stain-free technology on a Chemidoc MP. Proteins were then
1166 transferred to a nitrocellulose membrane and immunoblotted with anti-Bmh1 antibodies and then
1167 with anti-rabbit antibodies coupled to HRP, and revealed by chemiluminescence on a Chemidoc MP.
1168 The size difference is due to a longer linker present in the ymNeonGreen construct.* indicates the
1169 fluorescent species.

1170 Supplementary Figure 5. Spectral properties of red and orange fluorescent proteins
1171 used in this study.

1172 A. Excitation wavelengths of mCherry, TagRFP-T, mRuby2 and mKO-κ. Data were retrieved
1173 from FPBase (Lambert, 2019). The window of excitation provided by the Chemidoc MP
1174 imaging system is indicated in gray (520-545nm), the wavelength of the excitation laser of
1175 the Typhoon is indicated as a dotted line (532 nm), as per the manufacturer's indications.
1176 B. Emission wavelengths of mCherry, TagRFP-T, mRuby2 and mKO-κ. Data were retrieved
1177 from FPBase (Lambert, 2019). The window of emission collected by the Chemidoc MP
1178 system is indicated in gray (577-613nm), that of the Typhoon is indicated as shaded (≥550
1179 nm), as per the manufacturer's indications.

1180 Supplementary Figure 6. Effect of sample dilution on FP denaturation.

1181 A. Fluorescence of yeGFP is not maintained in LDS sample buffer at low protein concentrations.
1182 *Top*, Yeast expressing Bmh1-yeGFP were lysed in native conditions, samples were
1183 resuspended in LDS sample buffer, incubated for 5 min at 30°C and serially diluted (1:2) in
1184 LDS sample buffer. After migration, gels were imaged for green fluorescence using a
1185 Typhoon. Proteins were then transferred to a nitrocellulose membrane and immunoblotted
1186 with anti-Bmh1 antibodies and then with anti-rabbit antibodies coupled to HRP, and revealed
1187 by chemiluminescence on a Chemidoc MP. Red arrowhead: size of the native (fluorescent)
1188 protein; green arrowhead, size of the denatured protein. *Bottom*, Quantification of the signals
1189 obtained for fluorescence (black) and chemiluminescence (red: native protein, green:
1190 denatured protein) as a function of sample dilution. Linear-scaled and log-plot scaled graphs

1191 are shown. yeGFP denaturation increases with sample dilution, causing a bias when
1192 quantifying fluorescence.

1193 B. Design of the experiment to setup conditions to maintain FP fluorescence in diluted samples.
1194 Protein lysates prepared in native conditions from yeast expressing Bmh1-EGFP are diluted
1195 1:5 with dilution buffer (water, lysis buffer, NaCl at various concentrations, or 100 mM Tris-
1196 HCl solution at various pH) before mixing with 4X sample buffer pH6.8 (1X final
1197 concentration). Samples are then incubated at 50°C for 10 min before being loaded on SDS-
1198 PAGE.

1199 C. Effect of lysis buffer and NaCl concentration on in-gel fluorescence. Samples were diluted
1200 with water, native lysis buffer (1X, 0.75X, 0.5X or 0.25X in water) or NaCl solution (at the
1201 indicated concentration) before being incubated at 50°C for 10 min. After migration on a
1202 commercial precast 4-20%TGX gel (Bio-Rad), gels were imaged for green fluorescence
1203 using a Typhoon, and total proteins were visualized by the stain-free technology on a
1204 Chemidoc MP. Proteins were then transferred to a nitrocellulose membrane and
1205 immunoblotted with anti-GFP antibodies and then with anti-mouse antibodies coupled to
1206 HRP, and revealed by chemiluminescence on a Chemidoc MP.

1207 D. Effect of pH on in-gel fluorescence. Samples were diluted with native lysis buffer (1X), water
1208 or Tris-HCl 100 mM solution (final concentration) at the indicated pH before being incubated
1209 at 50°C for 10 min. After migration on a commercial precast 4-20%TGX gel (Bio-Rad), gels
1210 were imaged for green fluorescence using a Typhoon, and total proteins were visualized by
1211 the stain-free technology on a Chemidoc MP.

1212

1213 Supplementary Figure 7. Sensitivity and linearity of in-gel fluorescence detection of
1214 various FP

1215 A. Yeast expressing Bmh1-yeGFP were lysed in native conditions, samples were resuspended
1216 in LDS sample buffer and incubated for 5 min at 30°C. Samples were serially diluted (right
1217 to left) into sample buffer without LDS (see Material and Methods), and loaded onto SDS-
1218 PAGE. After migration, gels were imaged for fluorescence using a Typhoon. Quantification
1219 of the signals obtained for green fluorescence (black) and chemiluminescence (red) as a
1220 function of sample dilution (n=3 ± SD). Linear-scaled and log-plot scaled graphs are shown.

1221 B. Same as A, with Bmh1-sfGFP.

1222 C. Same as A, with Bmh1-mCherry.

1223 D. Same as A, with Bmh1-mKO- κ.

1224

1225 Supplementary Figure 8. Correlation of IGF signals with published abundances for
1226 various proteins and comparison with chemiluminescence detection.

1227 A. Correlation of IGF intensities with published abundance based on quantitative mass
1228 spectrometry experiments, western blot experiments, of confocal microscopy experiments.
1229 Data were from (Ho et al., 2018) and retrieved from SGD (www.yeastgenome.org) for
1230 untreated/unchallenged cells.
1231 B. Comparison of IGF with antibody-based chemiluminescence detection. The gels displayed
1232 in **Figure 7B** (also shown here on the top) were transferred onto a membrane and
1233 immunoblotted with the indicated antibodies for comparison.
1234

1235 Supplementary Figure 9. Bleedthrough of green fluorescence in the red fluorescence
1236 channel when using a Chemidoc MP.

1237 The same gel as that presented in **Figure 8A** was imaged for red fluorescence in a Chemidoc
1238 MP. * indicates the green fluorescent signal that is detected in the red channel.
1239

1240 Supplementary Figure 10. Endogenous fluorescent material in *C. elegans* worm
1241 extracts.

1242 A. Extended version of the gel presented in **Figure 9D**. Total protein extracts of *C. elegans*
1243 worms were prepared as detailed in *Material and Methods* and loaded onto precast TGX 4-
1244 20% gels (Bio-Rad). After migration, gels were imaged for fluorescence using a Typhoon
1245 at the indicated excitation/emission wavelengths. A fluorescent smear of unknown origin is
1246 visible in the green channel at around 250 kDa.
1247 B. The same samples as in A were loaded onto a precast TGX 4-20% gel (Bio-Rad) (left) or
1248 homemade 10% SDS-PAGE gel (right). After migration, gels were imaged for fluorescence
1249 using a Typhoon at the indicated excitation/emission wavelengths. The fluorescent smear
1250 in the green channel at around 250 kDa was no longer observed in homemade gels.
1251
1252
1253

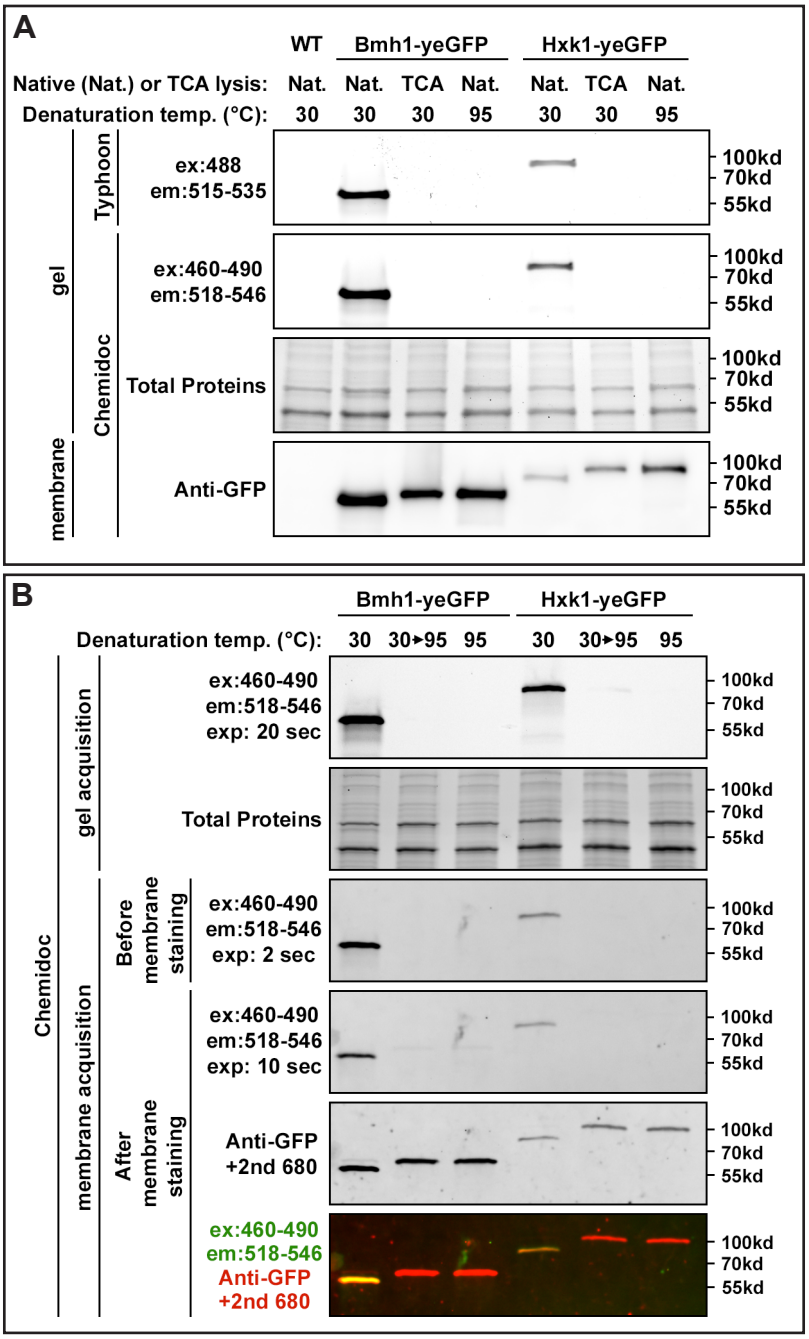
A
WT
Bmh1-yeGFP
Hxk1-yeGFP
Native (Nat.) or TCA lysis:
Nat. Nat. TCA Nat. Nat. TCA Nat.
Denaturation temp. (°C):
30 30 30 95 30 30 95
gel
membrane
Typhoon
Chemidoc
ex:488
em:515-535
ex:460-490
em:518-546
Total Proteins
Anti-GFP
100kd
70kd
55kd
B
Bmh1-yeGFP
Hxk1-yeGFP
Denaturation temp. (°C):
30 30▸95 95 30 30▸95 95
Chemidoc
gel acquisition
membrane acquisition
Before membrane staining
After membrane staining
ex:460-490
em:518-546
exp: 20 sec
Total Proteins
ex:460-490
em:518-546
exp: 2 sec
ex:460-490
em:518-546
exp: 10 sec
Anti-GFP
+2nd 680
ex:460-490
em:518-546
Anti-GFP
+2nd 680
100kd
70kd
55kd

Figure 1

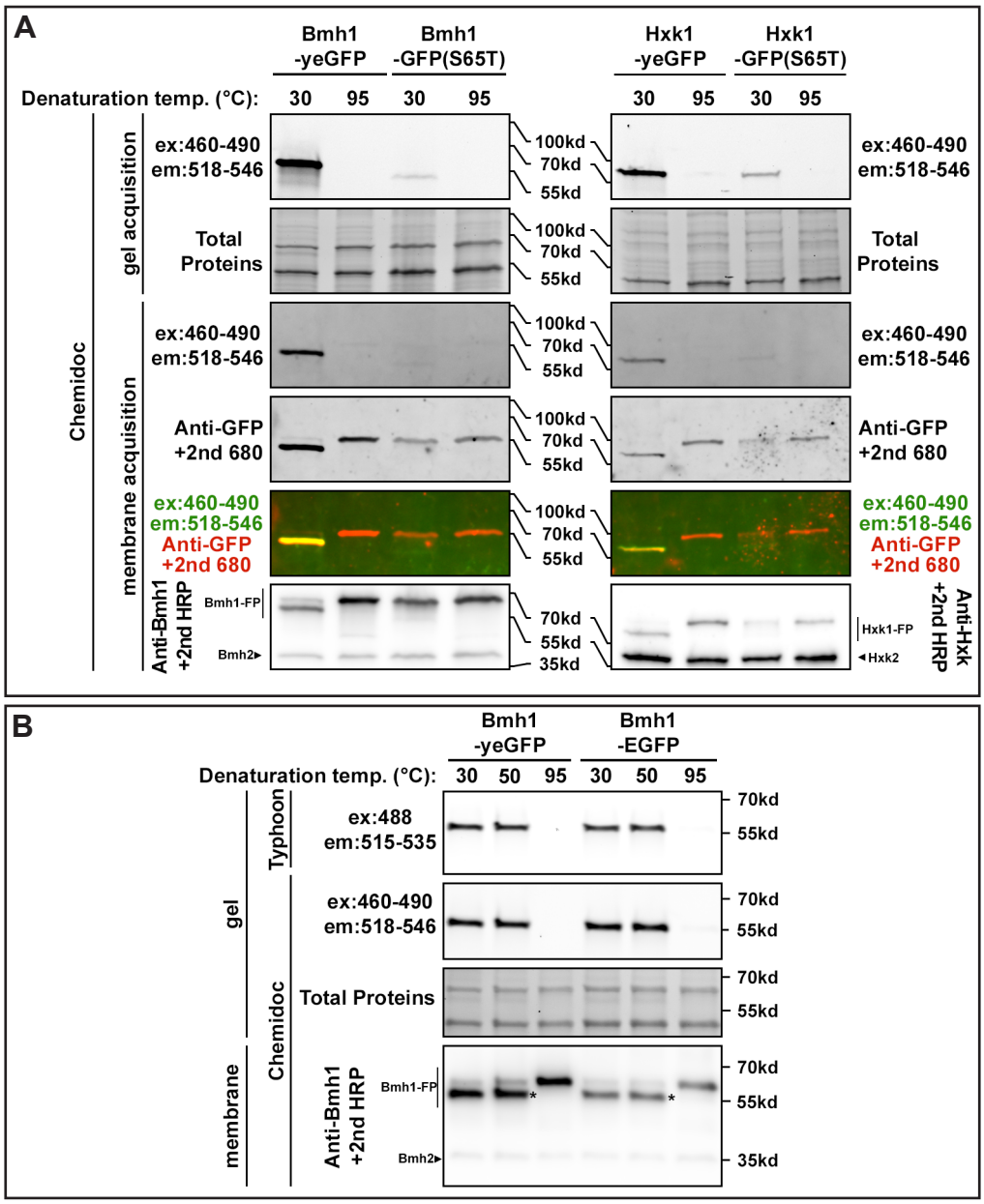
A
Bmh1 -yeGFP
Bmh1 -GFP(S65T)
Hxk1 -yeGFP
Hxk1 -GFP(S65T)
Denaturation temp. (°C):
30 95 30 95
30 95 30 95
Chemidoc
gel acquisition
membrane acquisition
ex:460-490 em:518-546
Total Proteins
Anti-GFP +2nd 680
ex:460-490 em:518-546 Anti-GFP +2nd 680
Anti-Bmh1 +2nd HRP
Anti-Hxk +2nd HRP
Bmh1-FP
Bmh2
Hxk1-FP
Hxk2
100kd
70kd
55kd
35kd
B
Bmh1 -yeGFP
Bmh1 -EGFP
Denaturation temp. (°C):
30 50 95 30 50 95
Typhoon
Chemidoc
gel
membrane
ex:488 em:515-535
ex:460-490 em:518-546
Total Proteins
Anti-Bmh1 +2nd HRP
Bmh1-FP
Bmh2
70kd
55kd
35kd

Figure 2

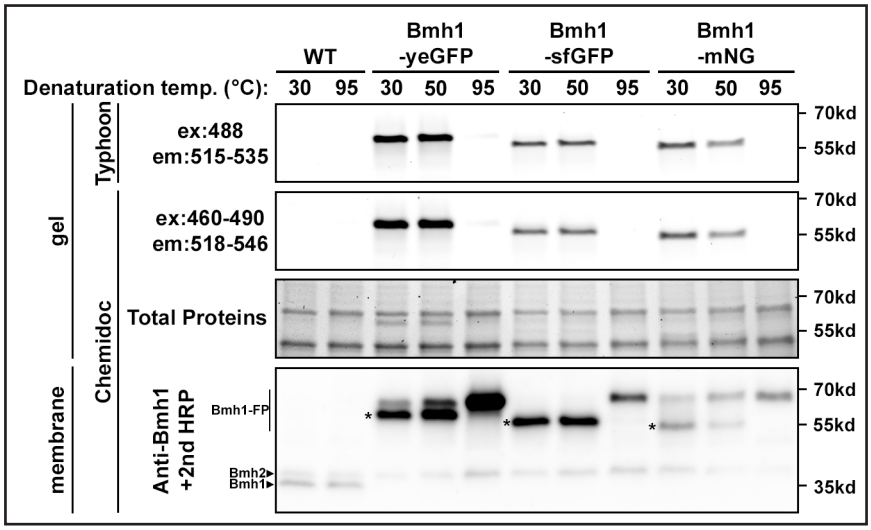
WT
Bmh1 -yeGFP
Bmh1 -sfGFP
Bmh1 -mNG
Denaturation temp. (°C): 30 95 30 50 95 30 50 95 30 50 95
gel
membrane
Typhoon
Chemidoc
ex:488 em:515-535
ex:460-490 em:518-546
Total Proteins
Anti-Bmh1 +2nd HRP
Bmh1-FP
Bmh2
Bmh1
70kd
55kd
35kd

Figure 3

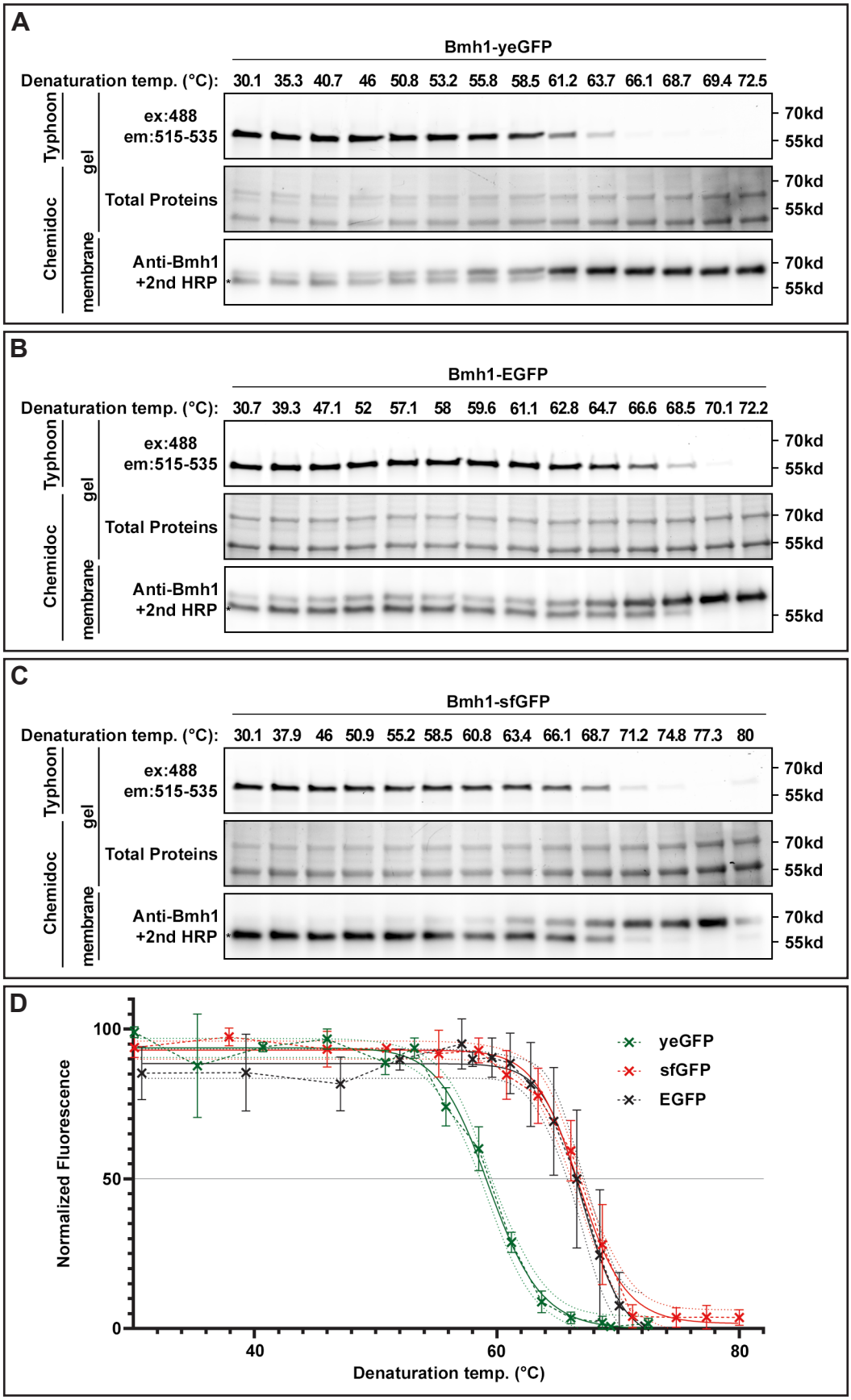
A
Bmh1-yeGFP
Denaturation temp. (°C): 30.1 35.3 40.7 46 50.8 53.2 55.8 58.5 61.2 63.7 66.1 68.7 69.4 72.5
Typhoon
Chemidoc
gel
membrane
ex:488
em:515-535
Total Proteins
Anti-Bmh1
+2nd HRP
70kd
55kd
B
Bmh1-EGFP
Denaturation temp. (°C): 30.7 39.3 47.1 52 57.1 58 59.6 61.1 62.8 64.7 66.6 68.5 70.1 72.2
C
Bmh1-sfGFP
Denaturation temp. (°C): 30.1 37.9 46 50.9 55.2 58.5 60.8 63.4 66.1 68.7 71.2 74.8 77.3 80
D
Normalized Fluorescence
Denaturation temp. (°C)
yeGFP
sfGFP
EGFP

Figure 4

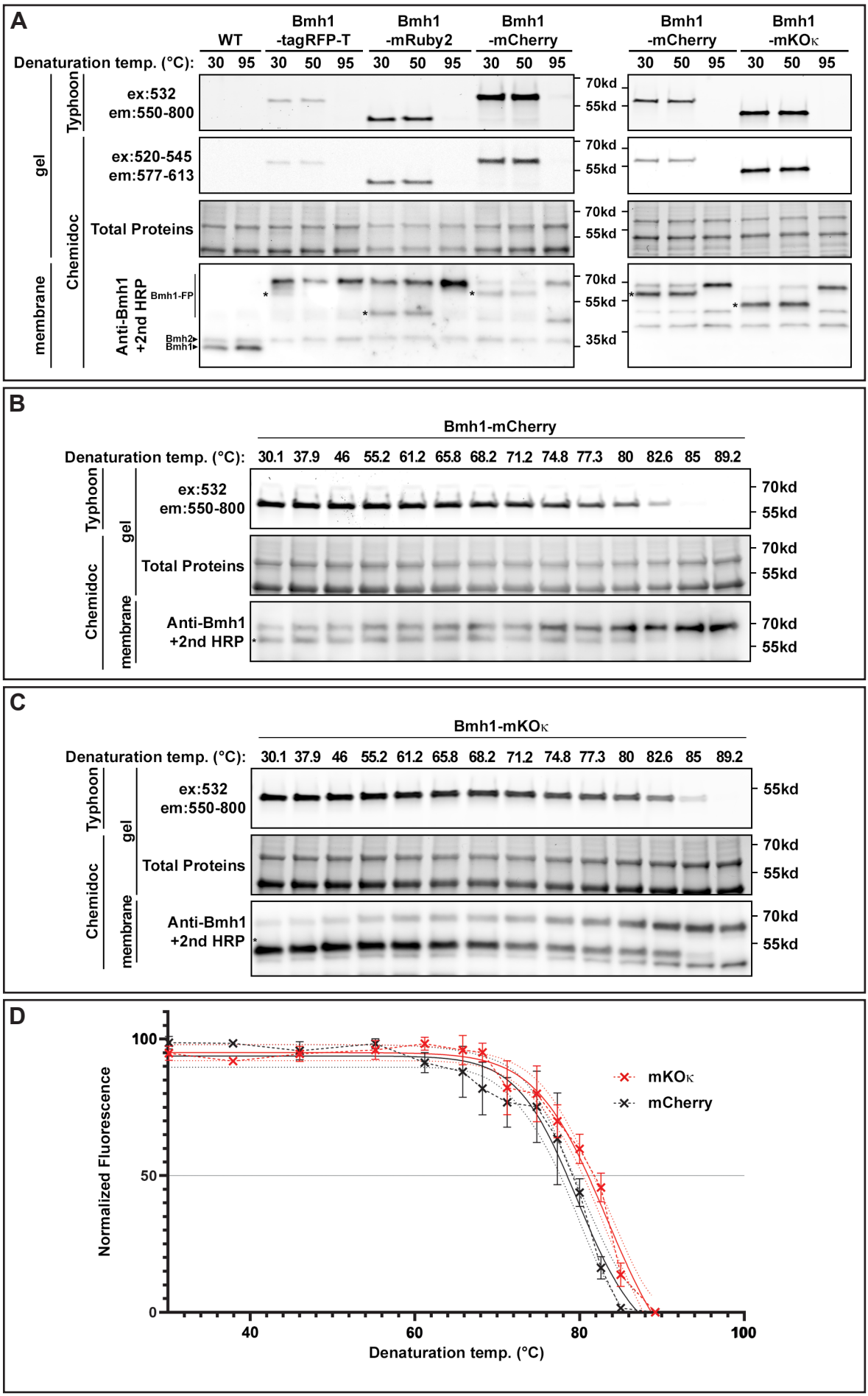
A
WT
Bmh1 -tagRFP-T
Bmh1 -mRuby2
Bmh1 -mCherry
Bmh1 -mCherry
Bmh1 -mKOκ
Denaturation temp. (°C): 30 95 30 50 95 30 50 95 30 50 95 30 50 95 30 50 95
gel
membrane
Typhoon
Chemidoc
ex:532 em:550-800
ex:520-545 em:577-613
Total Proteins
Anti-Bmh1 +2nd HRP
Bmh1-FP
Bmh2
Bmh1
70kd
55kd
35kd
B
Bmh1-mCherry
Denaturation temp. (°C): 30.1 37.9 46 55.2 61.2 65.8 68.2 71.2 74.8 77.3 80 82.6 85 89.2
Typhoon
Chemidoc
gel
membrane
ex:532 em:550-800
Total Proteins
Anti-Bmh1 +2nd HRP
70kd
55kd
C
Bmh1-mKOκ
Denaturation temp. (°C): 30.1 37.9 46 55.2 61.2 65.8 68.2 71.2 74.8 77.3 80 82.6 85 89.2
Typhoon
Chemidoc
gel
membrane
ex:532 em:550-800
Total Proteins
Anti-Bmh1 +2nd HRP
55kd
70kd
D
Normalized Fluorescence
Denaturation temp. (°C)
mKOκ
mCherry
0
50
100
40
60
80
100

Figure 5

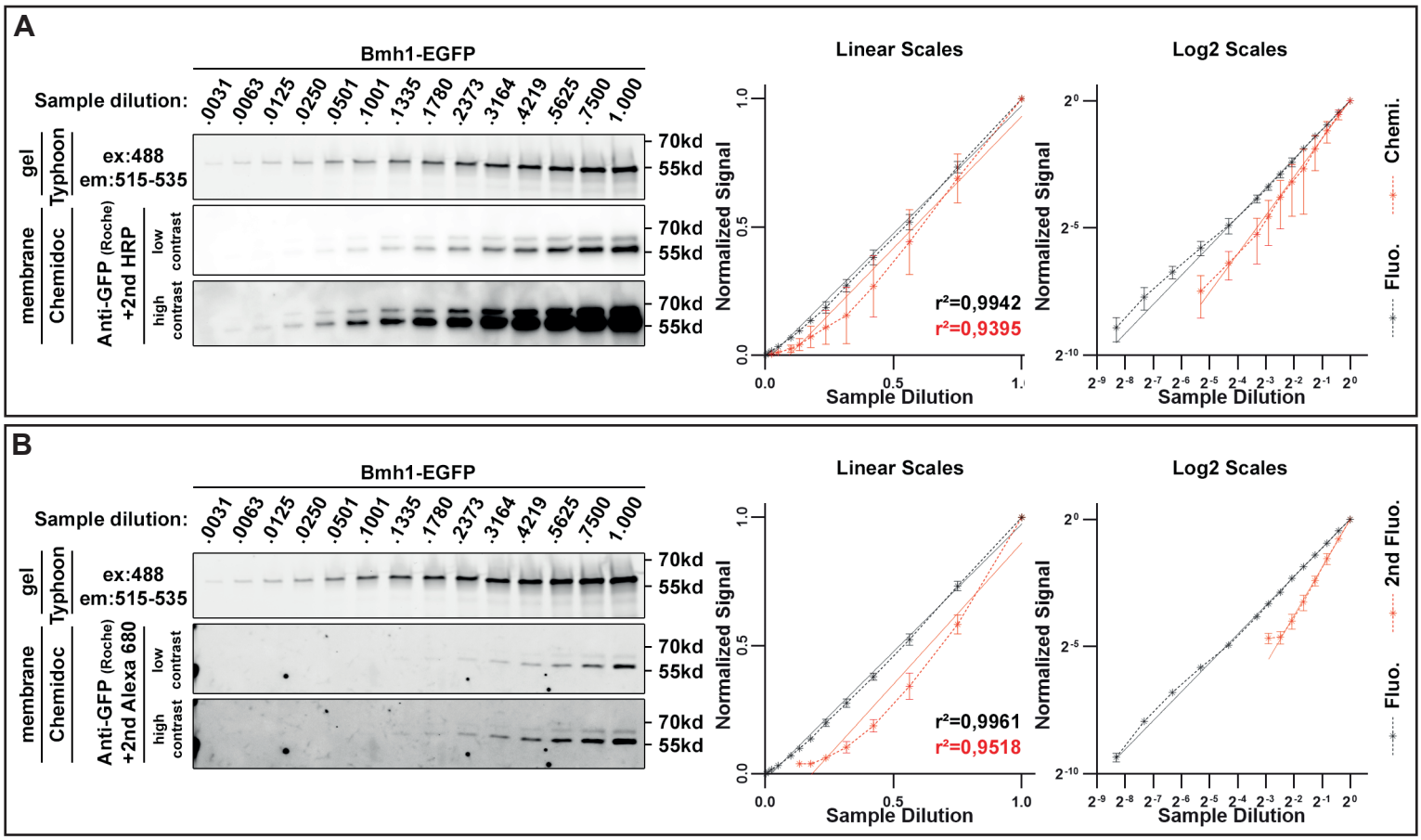
A
Bmh1-EGFP
Sample dilution:
.0031
.0063
.0125
.0250
.0501
.1001
.1335
.1780
.2373
.3164
.4219
.5625
.7500
1.000
gel
Typhoon
ex:488
em:515-535
membrane
Chemidoc
Anti-GFP (Roche)
+2nd HRP
low contrast
high contrast
70kd
55kd
Linear Scales
Log2 Scales
Normalized Signal
Sample Dilution
r²=0,9942
r²=0,9395
Chemi.
Fluo.
B
Anti-GFP (Roche)
+2nd Alexa 680
r²=0,9961
r²=0,9518
2nd Fluo.

Figure 6

A

Protein name	Localization	Features	Abundance (median)	MW (kd)
Kip3	Microtubules	Soluble	736	91,09
Hxt5	PM	Membrane	1060	66,251
Fkh1	Nuclear	Soluble	1771	53,49
Rod1	Cytosolic	Soluble	2171	92,349
Apl1	PM	Soluble	2237	80,453
mRpl25	Mitochondrial	Soluble, large complex	2403	18,587
Rtk1	Cytosolic	Soluble	3256	69,615
Reg1	Cytosolic	Soluble	4140	112,616
Sdh2	Mitochondrial	Soluble	5512	30,231
Snf1	Cytosolic	Soluble	5622	72,045
Ina1	PM	Membrane, glycosylated	7748	72,683
Rpa12	Nuclear	Soluble, large complex	11999	13,661
Ade16	Cytosolic	Soluble	12049	65,282
Spf1	ER membrane	Membrane	15064	135,269
Pre6	Cytosolic, nuclear	Soluble, large complex	16957	28,439
Ipp1	Cytosolic	Soluble	42812	32,3
Bmh1	Cytosolic, nuclear	Soluble	65471	30,091

C

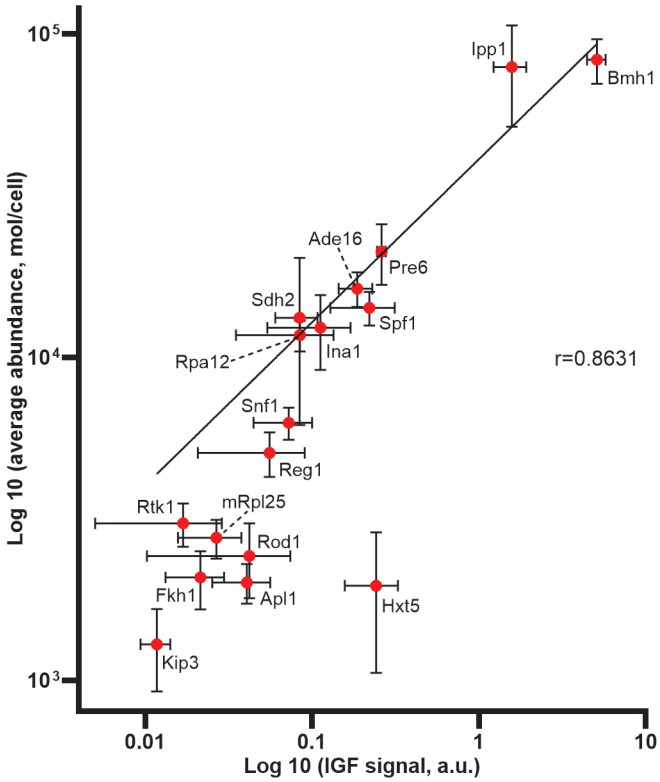

B

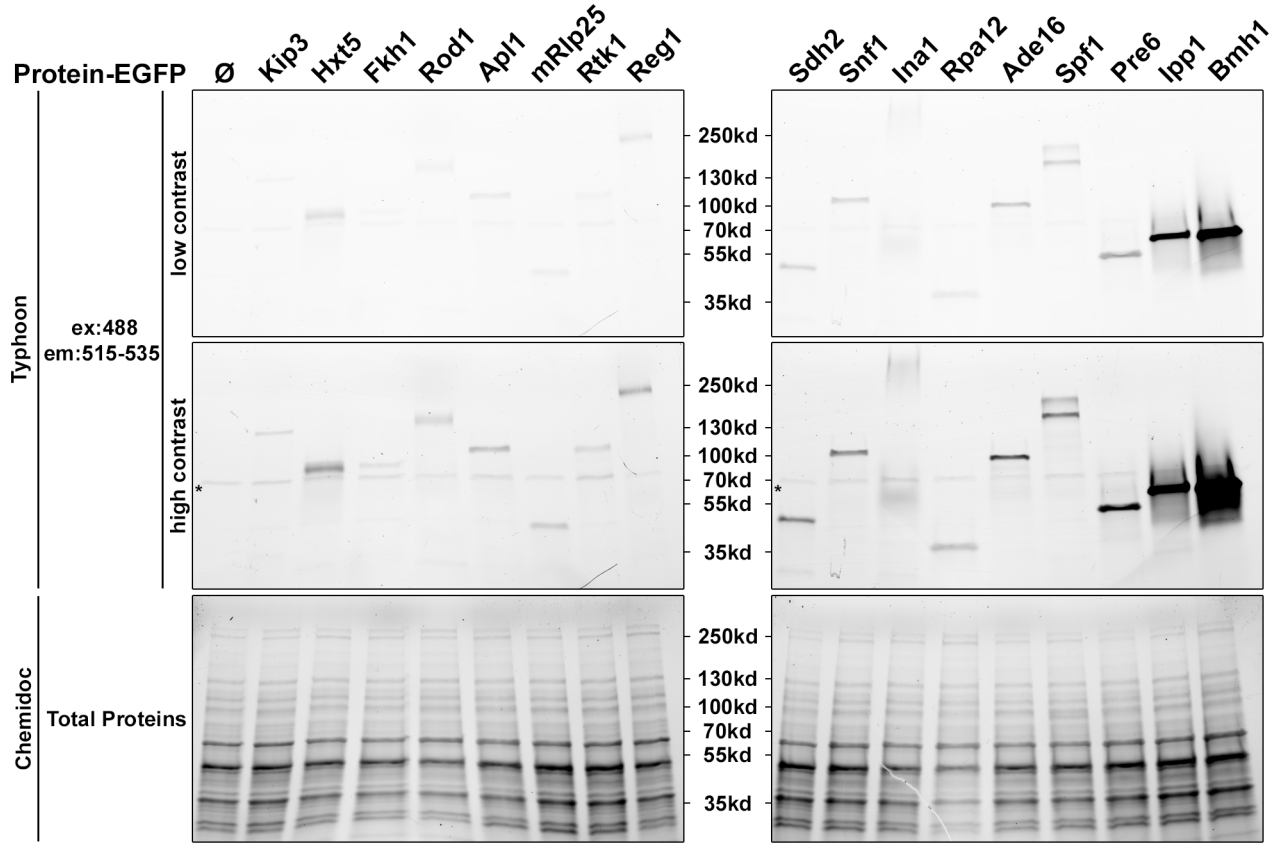

Figure 7

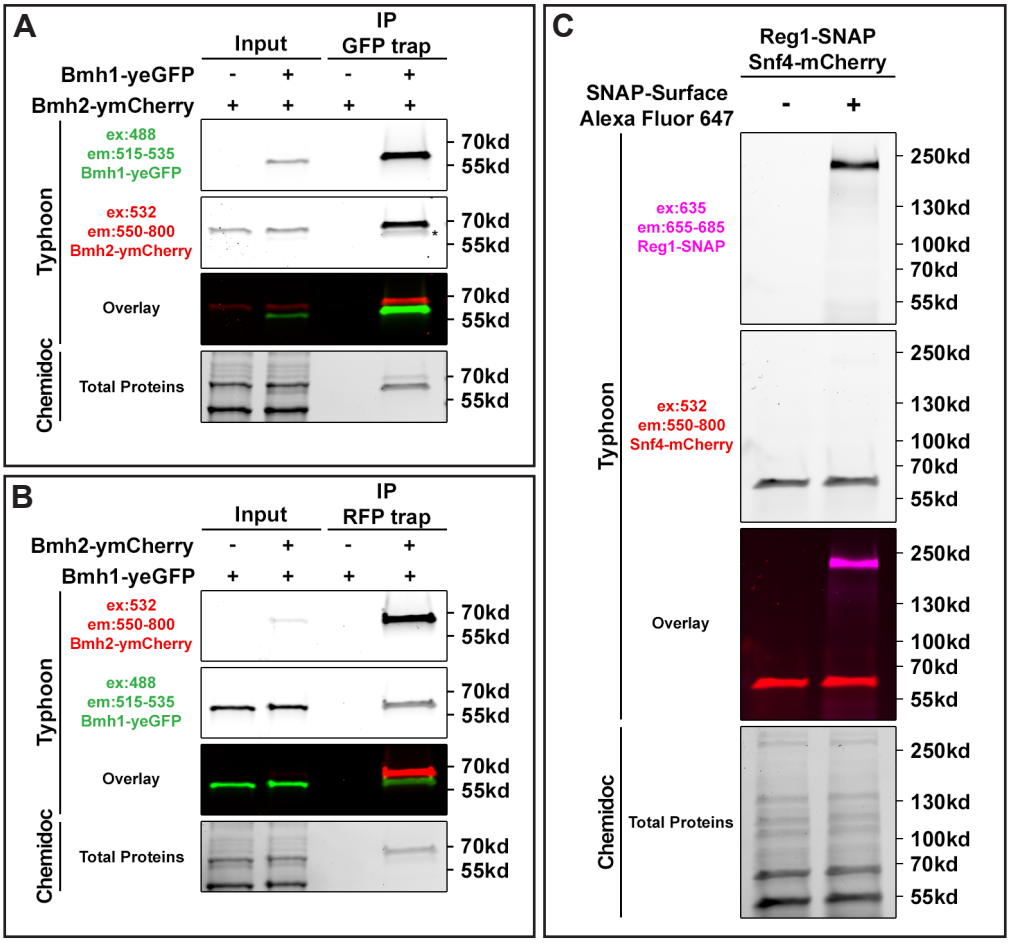
A
Input
IP
GFP trap
Bmh1-yeGFP
Bmh2-ymCherry
Typhoon
Chemidoc
ex:488
em:515-535
Bmh1-yeGFP
ex:532
em:550-800
Bmh2-ymCherry
Overlay
Total Proteins
70kd
55kd
B
Input
IP
RFP trap
Bmh2-ymCherry
Bmh1-yeGFP
Typhoon
Chemidoc
ex:532
em:550-800
Bmh2-ymCherry
ex:488
em:515-535
Bmh1-yeGFP
Overlay
Total Proteins
70kd
55kd
C
Reg1-SNAP
Snf4-mCherry
SNAP-Surface
Alexa Fluor 647
Typhoon
Chemidoc
ex:635
em:655-685
Reg1-SNAP
ex:532
em:550-800
Snf4-mCherry
Overlay
Total Proteins
250kd
130kd
100kd
70kd
55kd

Figure 8

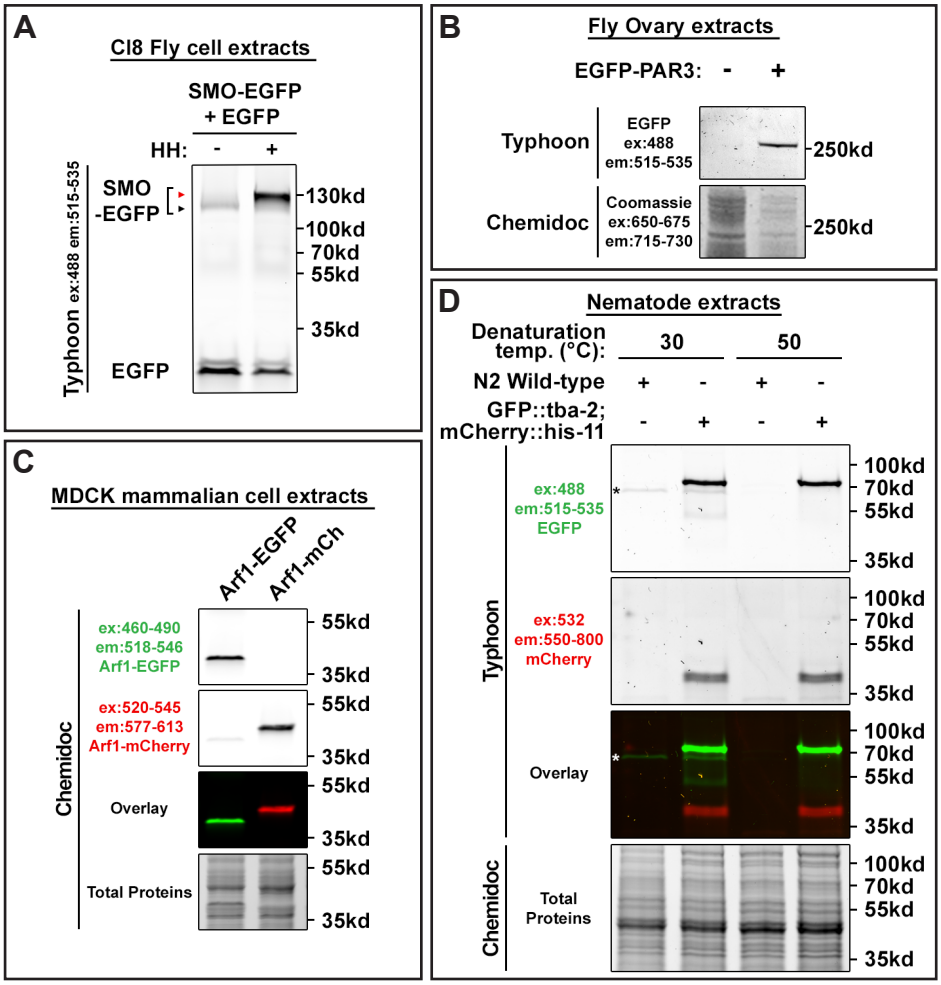
A
Cl8 Fly cell extracts
SMO-EGFP
+ EGFP
HH: - +
Typhoon ex:488 em:515-535
SMO
-EGFP
EGFP
130kd
100kd
70kd
55kd
35kd
B
Fly Ovary extracts
EGFP-PAR3: - +
Typhoon
EGFP
ex:488
em:515-535
250kd
Chemidoc
Coomassie
ex:650-675
em:715-730
250kd
C
MDCK mammalian cell extracts
Arf1-EGFP
Arf1-mCh
Chemidoc
ex:460-490
em:518-546
Arf1-EGFP
ex:520-545
em:577-613
Arf1-mCherry
Overlay
Total Proteins
55kd
35kd
D
Nematode extracts
Denaturation temp. (°C): 30 50
N2 Wild-type + - + -
GFP::tba-2; mCherry::his-11 - + - +
Typhoon
ex:488
em:515-535
EGFP
ex:532
em:550-800
mCherry
Overlay
Chemidoc
Total Proteins
100kd
70kd
55kd
35kd

Figure 9

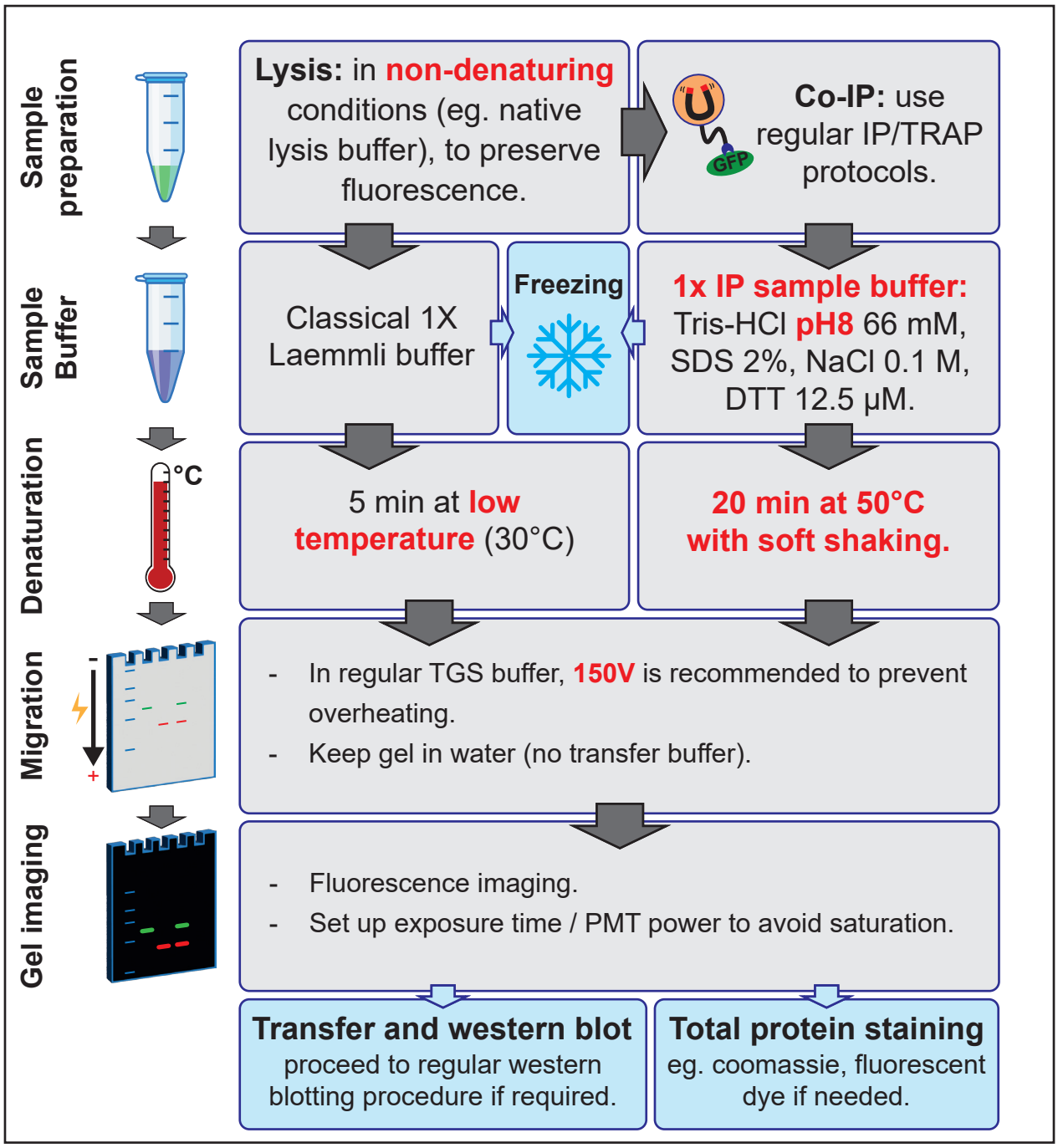
Sample preparation
Lysis: in non-denaturing conditions (eg. native lysis buffer), to preserve fluorescence.
GFP
Co-IP: use regular IP/TRAP protocols.
Sample Buffer
Classical 1X Laemmli buffer
Freezing
1x IP sample buffer: Tris-HCl pH8 66 mM, SDS 2%, NaCl 0.1 M, DTT 12.5 µM.
Denaturation
°C
5 min at low temperature (30°C)
20 min at 50°C with soft shaking.
Migration
- In regular TGS buffer, 150V is recommended to prevent overheating.
- Keep gel in water (no transfer buffer).
Gel imaging
- Fluorescence imaging.
- Set up exposure time / PMT power to avoid saturation.
Transfer and western blot
proceed to regular western blotting procedure if required.
Total protein staining
eg. coomassie, fluorescent dye if needed.

Figure 10

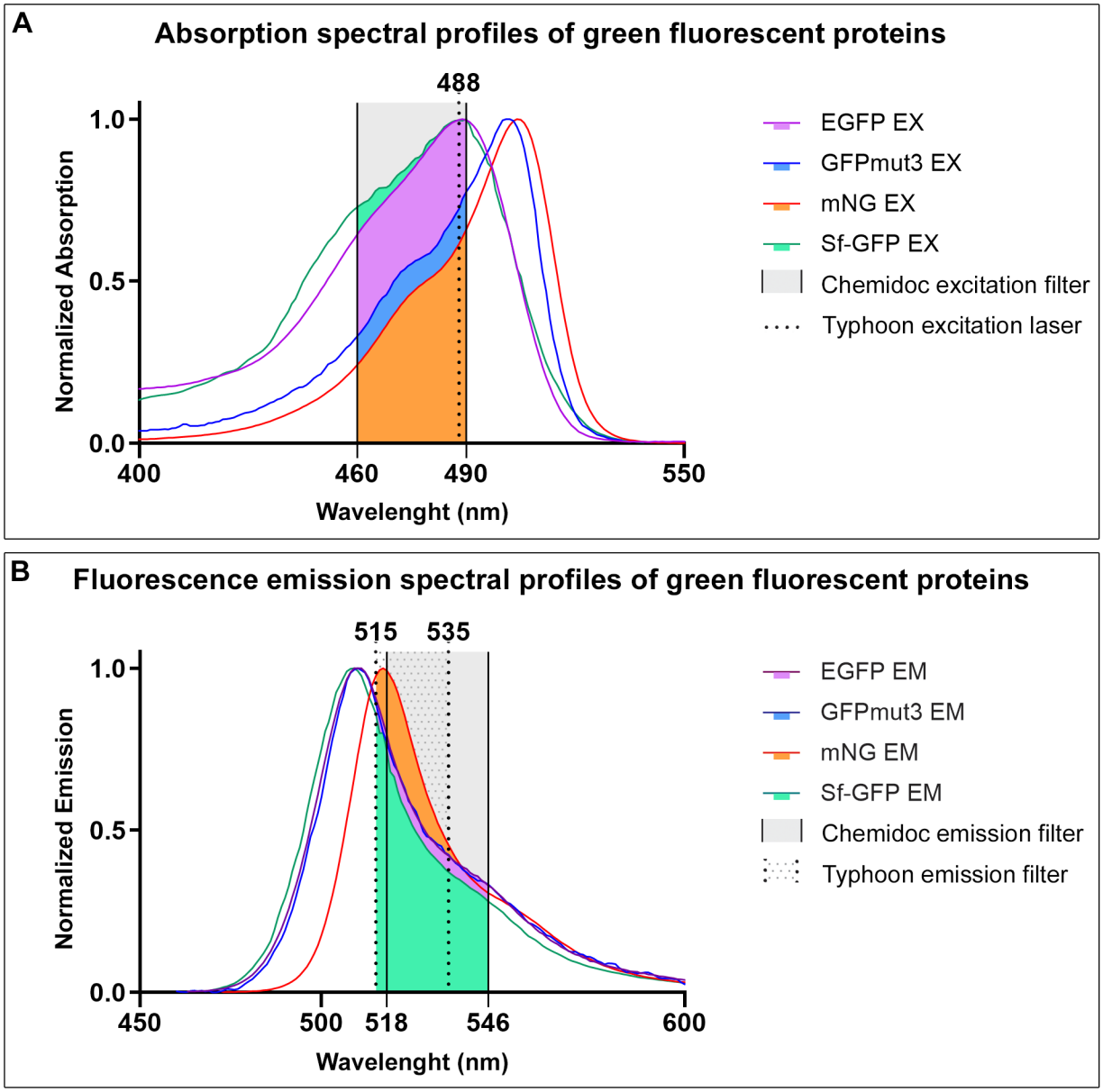
A
Absorption spectral profiles of green fluorescent proteins
488
1.0
0.5
0.0
Normalized Absorption
400
460
490
550
Wavelenght (nm)
EGFP EX
GFPmut3 EX
mNG EX
Sf-GFP EX
Chemidoc excitation filter
Typhoon excitation laser
B
Fluorescence emission spectral profiles of green fluorescent proteins
515
535
1.0
0.5
0.0
Normalized Emission
450
500
518
546
600
Wavelenght (nm)
EGFP EM
GFPmut3 EM
mNG EM
Sf-GFP EM
Chemidoc emission filter
Typhoon emission filter

Figure S1

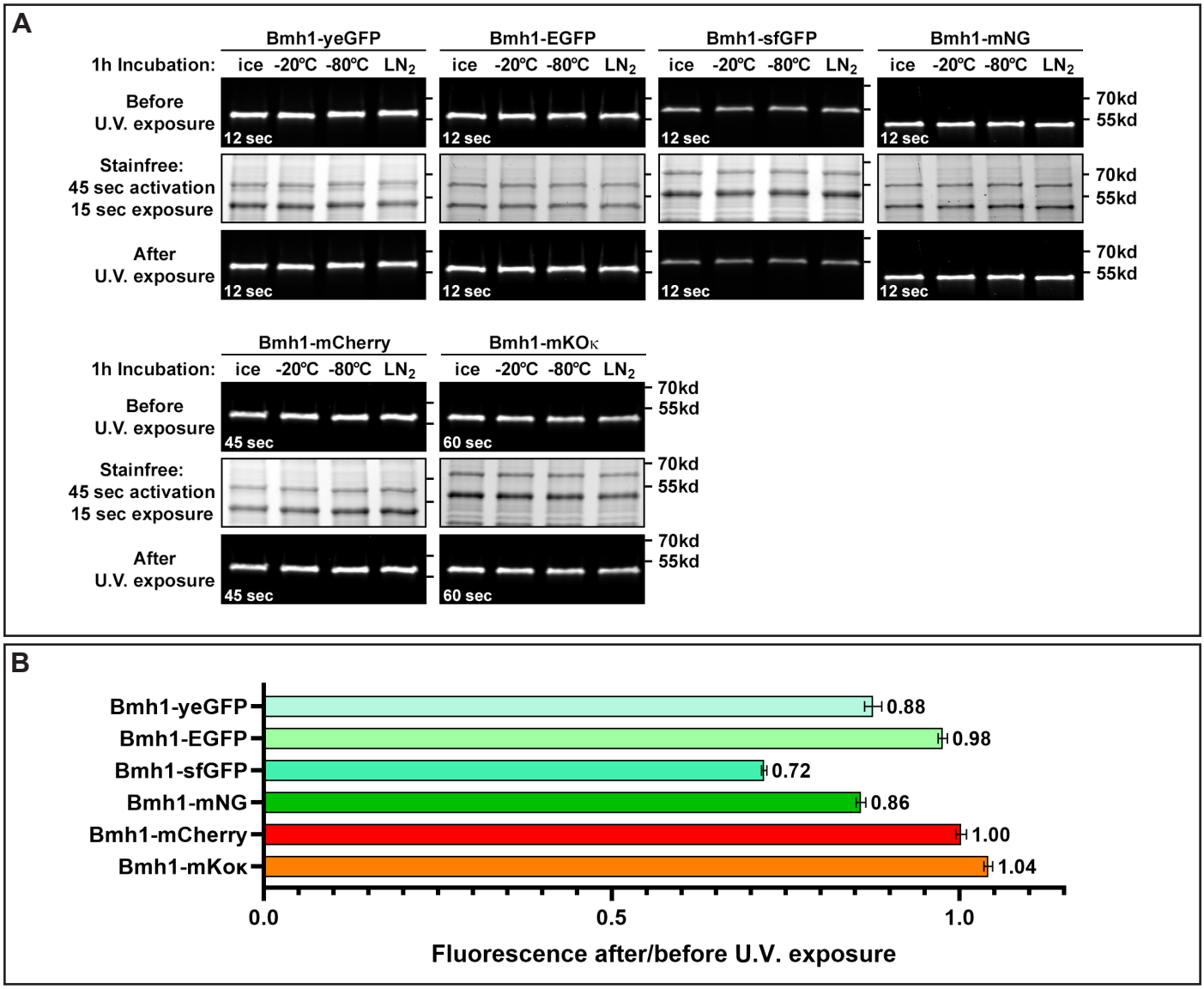
A
Bmh1-yeGFP
Bmh1-EGFP
Bmh1-sfGFP
Bmh1-mNG
1h Incubation:
ice -20°C -80°C LN2
Before U.V. exposure
Stainfree: 45 sec activation 15 sec exposure
After U.V. exposure
12 sec
70kd
55kd
Bmh1-mCherry
Bmh1-mKOκ
45 sec
60 sec

B
Bmh1-yeGFP
Bmh1-EGFP
Bmh1-sfGFP
Bmh1-mNG
Bmh1-mCherry
Bmh1-mKoκ
0.88
0.98
0.72
0.86
1.00
1.04
0.0
0.5
1.0
Fluorescence after/before U.V. exposure

Figure S2

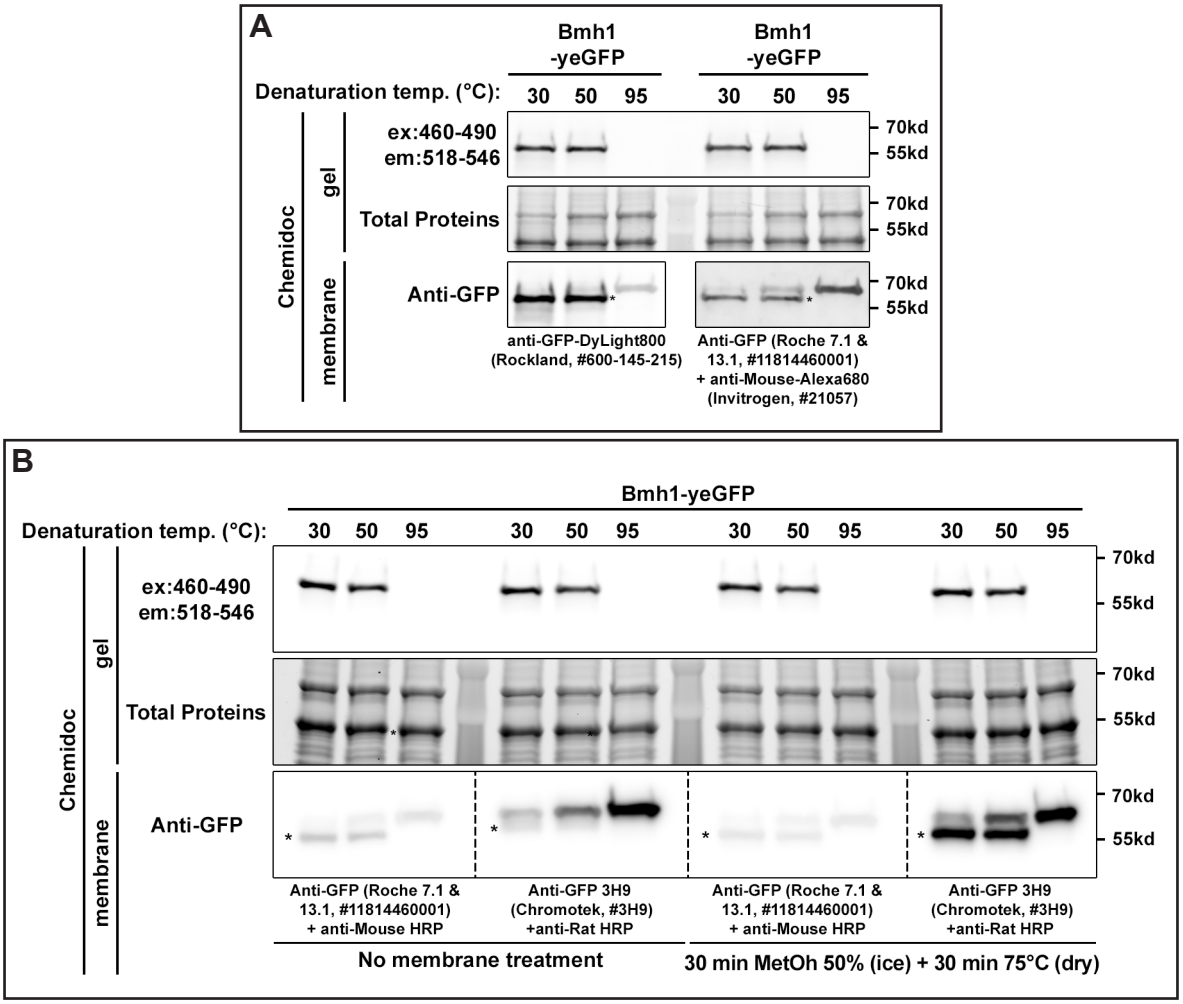
A
Bmh1 -yeGFP
Bmh1 -yeGFP
Denaturation temp. (°C):
30 50 95
30 50 95
Chemidoc
gel
membrane
ex:460-490
em:518-546
Total Proteins
Anti-GFP
70kd
55kd
anti-GFP-DyLight800 (Rockland, #600-145-215)
Anti-GFP (Roche 7.1 & 13.1, #11814460001) + anti-Mouse-Alexa680 (Invitrogen, #21057)
B
Bmh1-yeGFP
Denaturation temp. (°C):
30 50 95 30 50 95 30 50 95 30 50 95
Chemidoc
gel
membrane
ex:460-490
em:518-546
Total Proteins
Anti-GFP
70kd
55kd
Anti-GFP (Roche 7.1 & 13.1, #11814460001) + anti-Mouse HRP
Anti-GFP 3H9 (Chromotek, #3H9) +anti-Rat HRP
Anti-GFP (Roche 7.1 & 13.1, #11814460001) + anti-Mouse HRP
Anti-GFP 3H9 (Chromotek, #3H9) +anti-Rat HRP
No membrane treatment
30 min MetOh 50% (ice) + 30 min 75°C (dry)

Figure S3

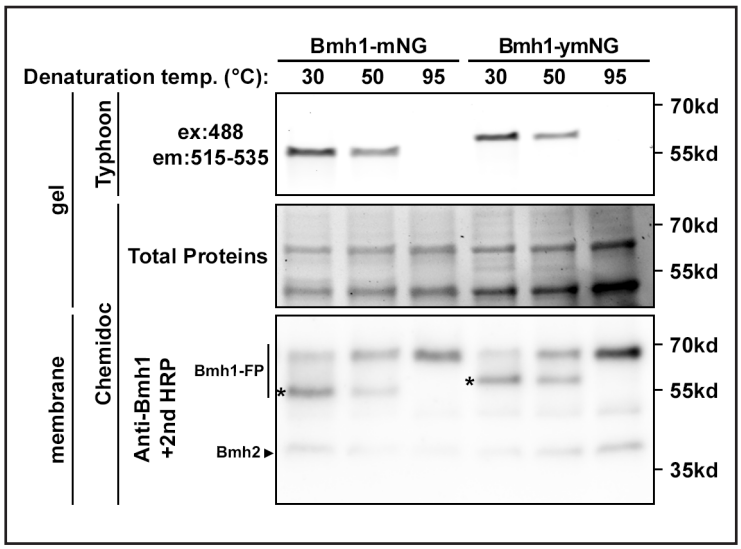
Bmh1-mNG
Bmh1-ymNG
Denaturation temp. (°C):
30
50
95
30
50
95
gel
Typhoon
ex:488
em:515-535
70kd
55kd
Chemidoc
Total Proteins
70kd
55kd
membrane
Anti-Bmh1
+2nd HRP
Bmh1-FP
*
*
Bmh2
70kd
55kd
35kd

Figure S4

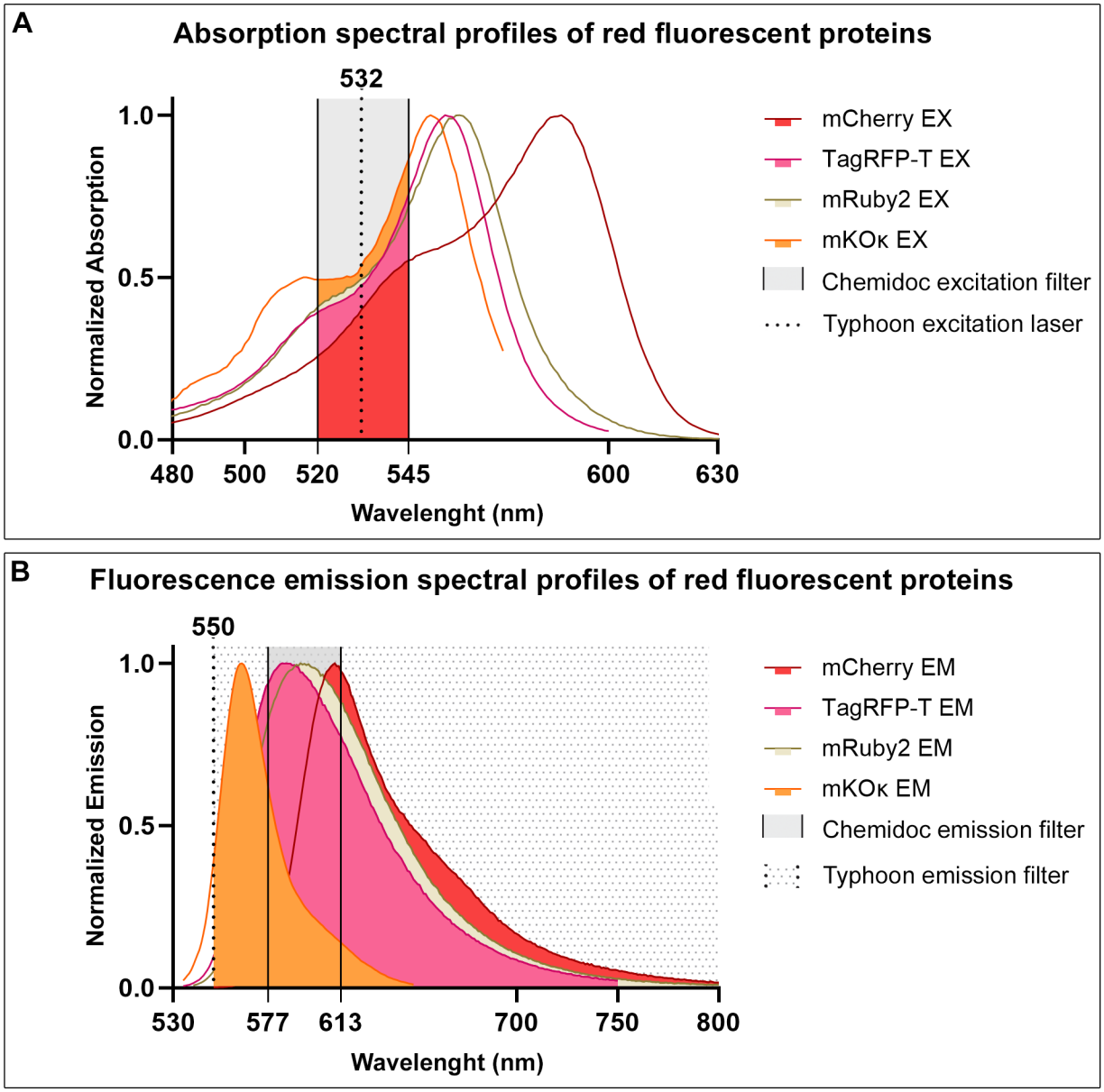
A
Absorption spectral profiles of red fluorescent proteins
532
1.0
0.5
0.0
Normalized Absorption
480
500
520
545
600
630
Wavelenght (nm)
mCherry EX
TagRFP-T EX
mRuby2 EX
mKOκ EX
Chemidoc excitation filter
Typhoon excitation laser
B
Fluorescence emission spectral profiles of red fluorescent proteins
550
1.0
0.5
0.0
Normalized Emission
530
577
613
700
750
800
Wavelenght (nm)
mCherry EM
TagRFP-T EM
mRuby2 EM
mKOκ EM
Chemidoc emission filter
Typhoon emission filter

Figure S5

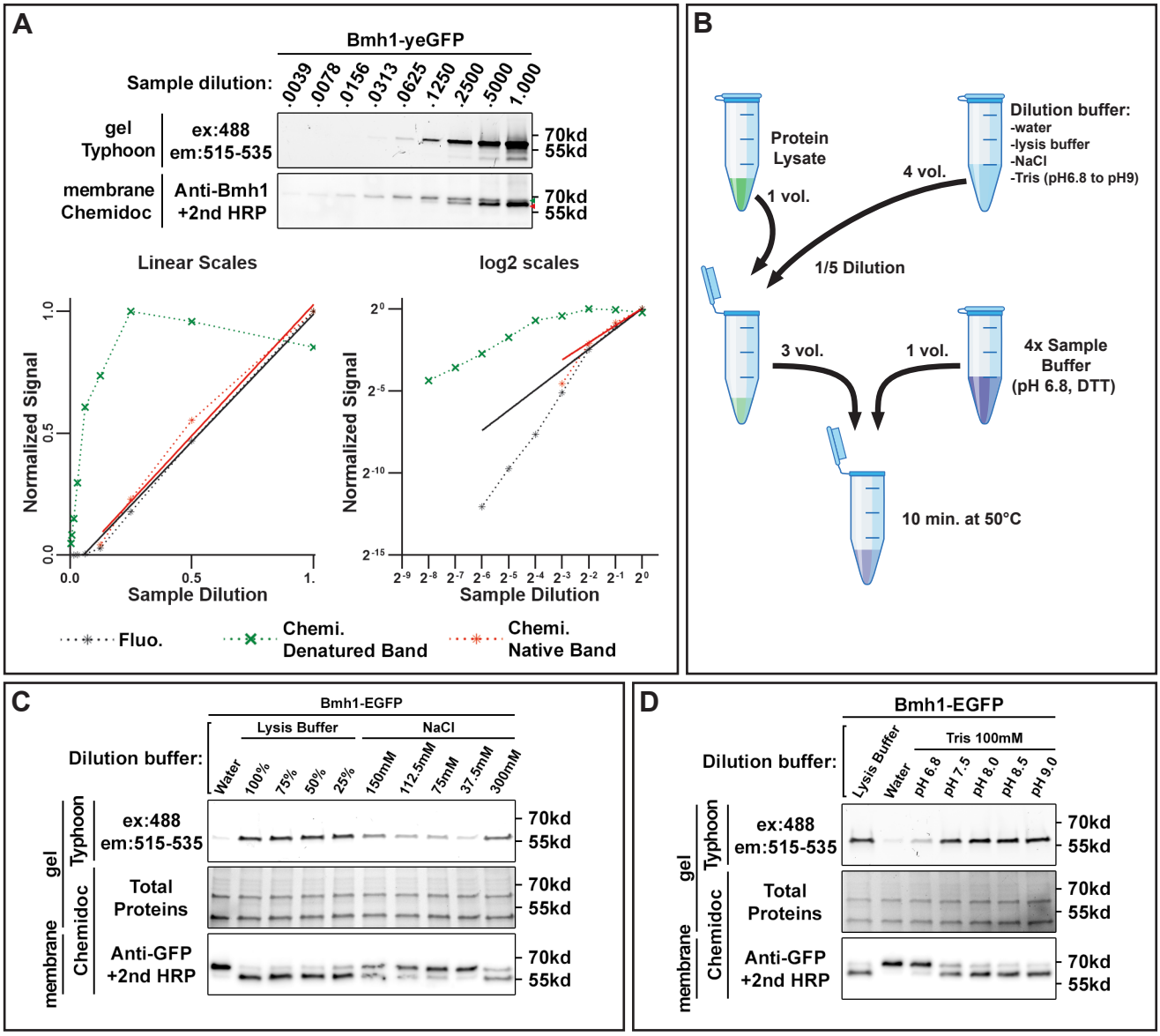
A
Bmh1-yeGFP
Sample dilution:
.0039
.0078
.0156
.0313
.0625
.1250
.2500
.5000
1.000
gel
Typhoon
ex:488
em:515-535
70kd
55kd
membrane
Chemidoc
Anti-Bmh1
+2nd HRP
70kd
55kd
Linear Scales
log2 scales
Normalized Signal
Sample Dilution
Fluo.
Chemi.
Denatured Band
Chemi.
Native Band
B
Protein
Lysate
1 vol.
4 vol.
Dilution buffer:
-water
-lysis buffer
-NaCl
-Tris (pH6.8 to pH9)
1/5 Dilution
3 vol.
1 vol.
4x Sample
Buffer
(pH 6.8, DTT)
10 min. at 50°C
C
Bmh1-EGFP
Dilution buffer:
Lysis Buffer
NaCl
Water
100%
75%
50%
25%
150mM
112.5mM
75mM
37.5mM
300mM
gel
Typhoon
ex:488
em:515-535
membrane
Chemidoc
Total
Proteins
Anti-GFP
+2nd HRP
70kd
55kd
D
Bmh1-EGFP
Dilution buffer:
Lysis Buffer
Tris 100mM
Water
pH 6.8
pH 7.5
pH 8.0
pH 8.5
pH 9.0
gel
Typhoon
ex:488
em:515-535
membrane
Chemidoc
Total
Proteins
Anti-GFP
+2nd HRP
70kd
55kd

Figure S6

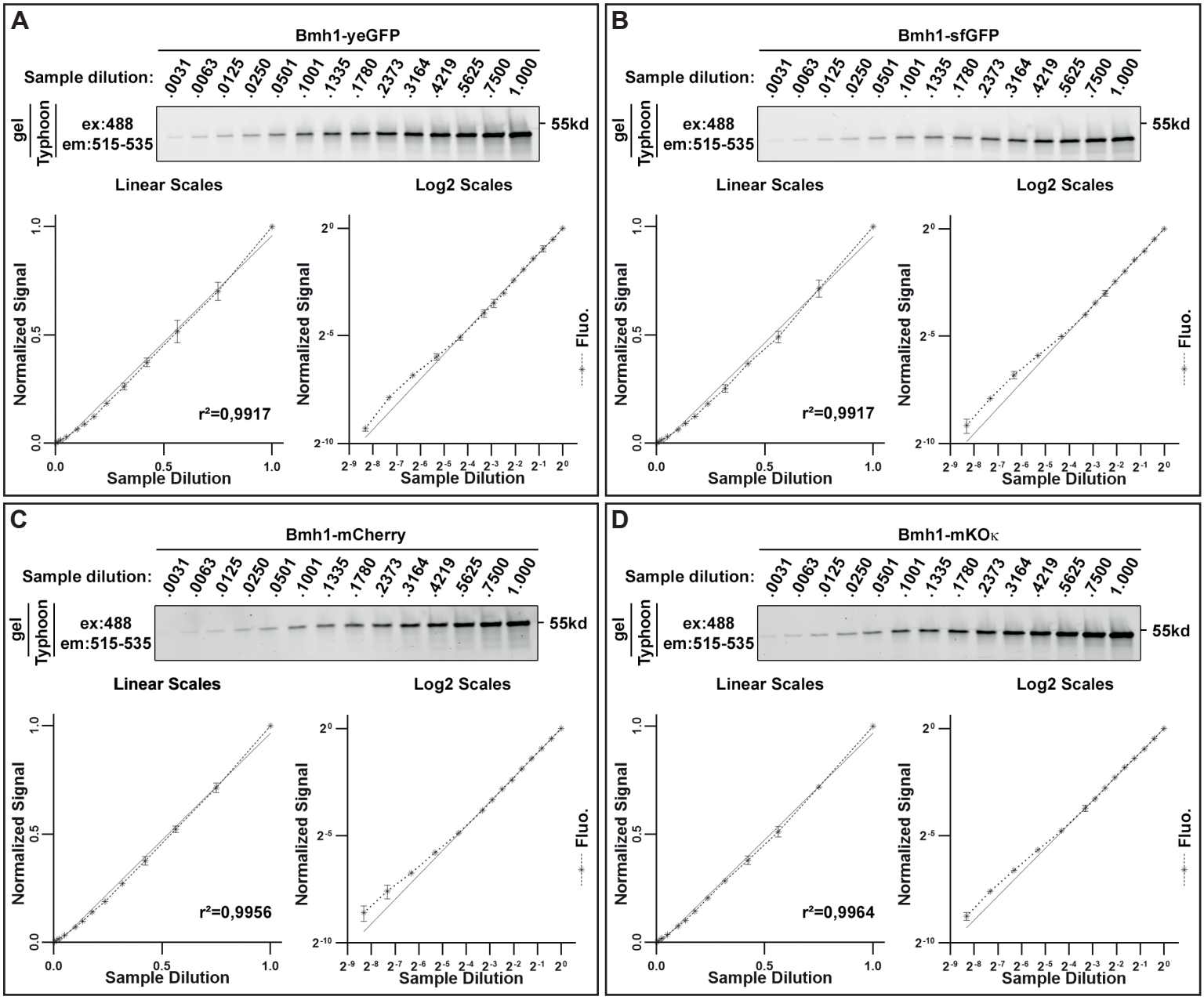
A
Bmh1-yeGFP
Sample dilution: .0031 .0063 .0125 .0250 .0501 .1001 .1335 .1780 .2373 .3164 .4219 .5625 .7500 1.000
gel Typhoon
ex:488
em:515-535
55kd
Linear Scales
Log2 Scales
Normalized Signal
Sample Dilution
r²=0,9917
Fluo.
B
Bmh1-sfGFP
Sample dilution: .0031 .0063 .0125 .0250 .0501 .1001 .1335 .1780 .2373 .3164 .4219 .5625 .7500 1.000
gel Typhoon
ex:488
em:515-535
55kd
Linear Scales
Log2 Scales
Normalized Signal
Sample Dilution
r²=0,9917
Fluo.
C
Bmh1-mCherry
Sample dilution: .0031 .0063 .0125 .0250 .0501 .1001 .1335 .1780 .2373 .3164 .4219 .5625 .7500 1.000
gel Typhoon
ex:488
em:515-535
55kd
Linear Scales
Log2 Scales
Normalized Signal
Sample Dilution
r²=0,9956
Fluo.
D
Bmh1-mKOκ
Sample dilution: .0031 .0063 .0125 .0250 .0501 .1001 .1335 .1780 .2373 .3164 .4219 .5625 .7500 1.000
gel Typhoon
ex:488
em:515-535
55kd
Linear Scales
Log2 Scales
Normalized Signal
Sample Dilution
r²=0,9964
Fluo.

Figure S7

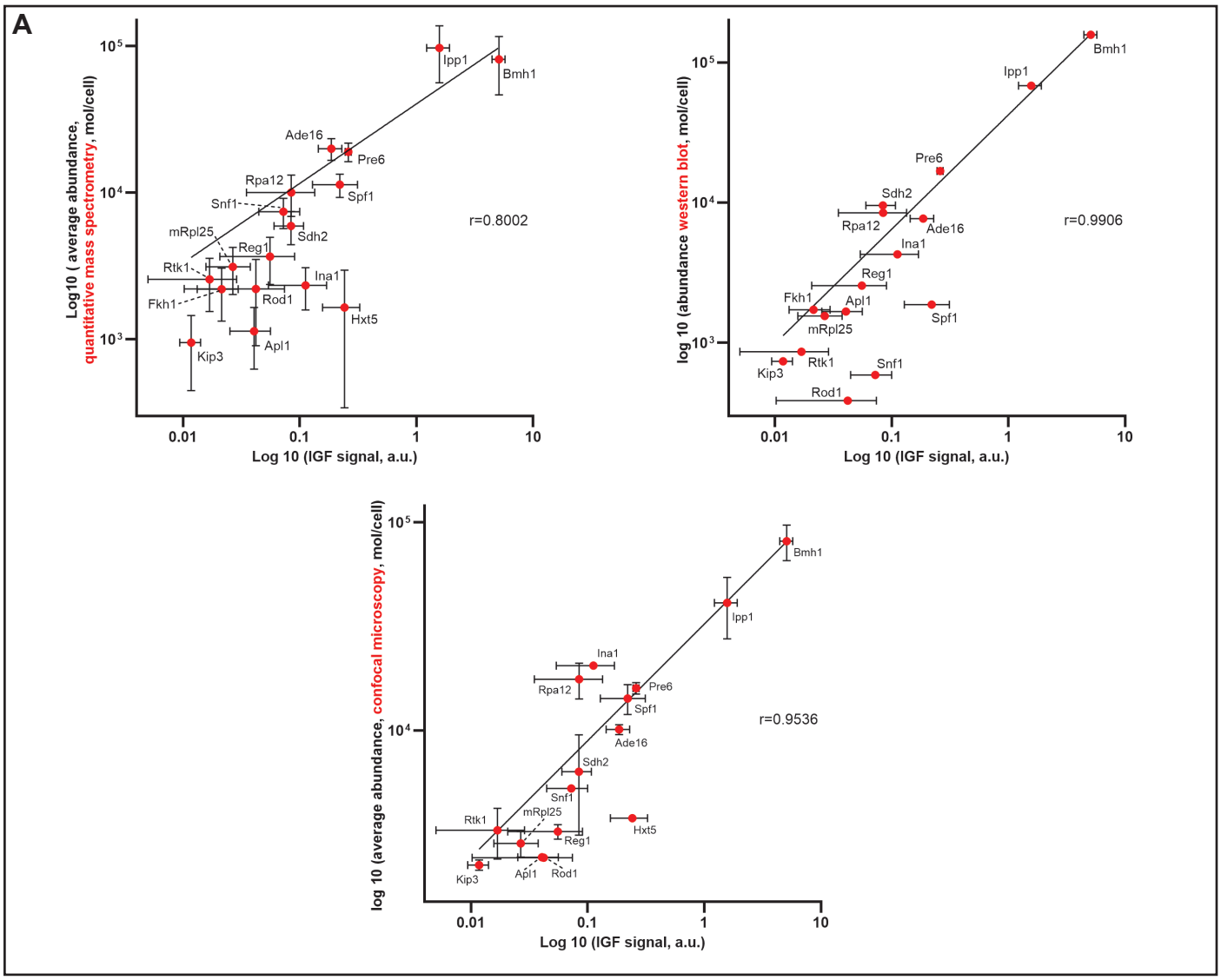
A
Log10 (average abundance, quantitative mass spectrometry, mol/cell)
Log 10 (IGF signal, a.u.)
r=0.8002
log 10 (abundance western blot, mol/cell)
r=0.9906
log 10 (average abundance, confocal microscopy, mol/cell)
r=0.9536
Ipp1
Bmh1
Ade16
Pre6
Rpa12
Spf1
Snf1
Sdh2
mRpl25
Reg1
Rtk1
Ina1
Fkh1
Rod1
Hxt5
Kip3
Apl1

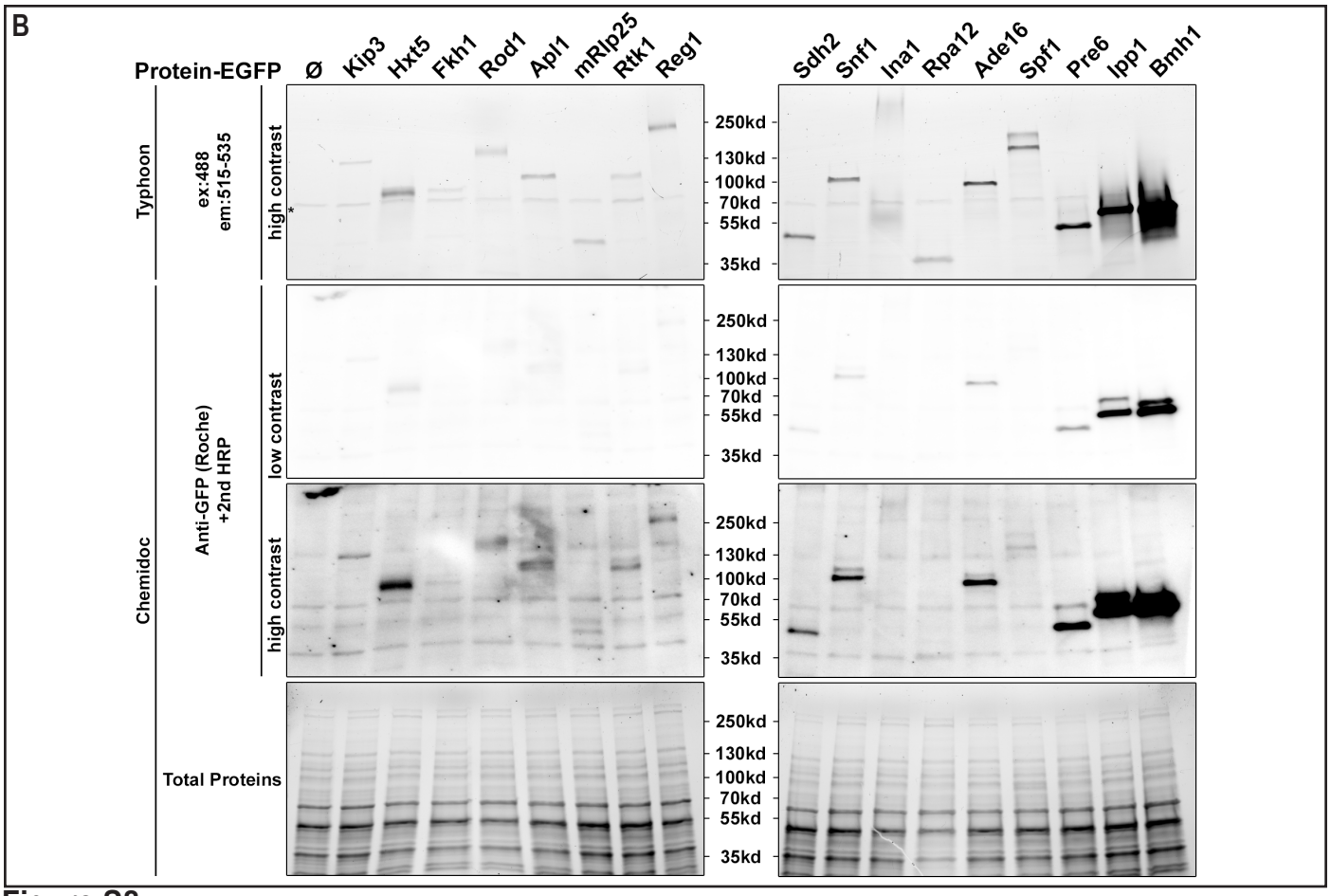
B
Protein-EGFP
Ø
Kip3
Hxt5
Fkh1
Rod1
Apl1
mRlp25
Rtk1
Reg1
Sdh2
Snf1
Ina1
Rpa12
Ade16
Spf1
Pre6
Ipp1
Bmh1
Typhoon
ex:488
em:515-535
high contrast
Chemidoc
Anti-GFP (Roche)
+2nd HRP
low contrast
high contrast
Total Proteins
250kd
130kd
100kd
70kd
55kd
35kd

Figure S8

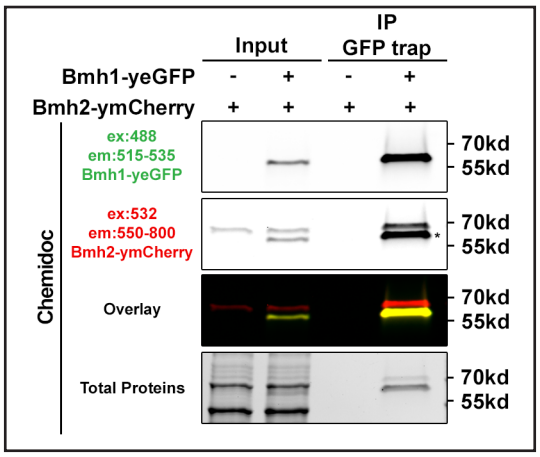
Input
IP
GFP trap
Bmh1-yeGFP
- + - +
Bmh2-ymCherry
+ + + +
Chemidoc
ex:488
em:515-535
Bmh1-yeGFP
ex:532
em:550-800
Bmh2-ymCherry
Overlay
Total Proteins
70kd
55kd
70kd
55kd
70kd
55kd
70kd
55kd
*

Figure S9

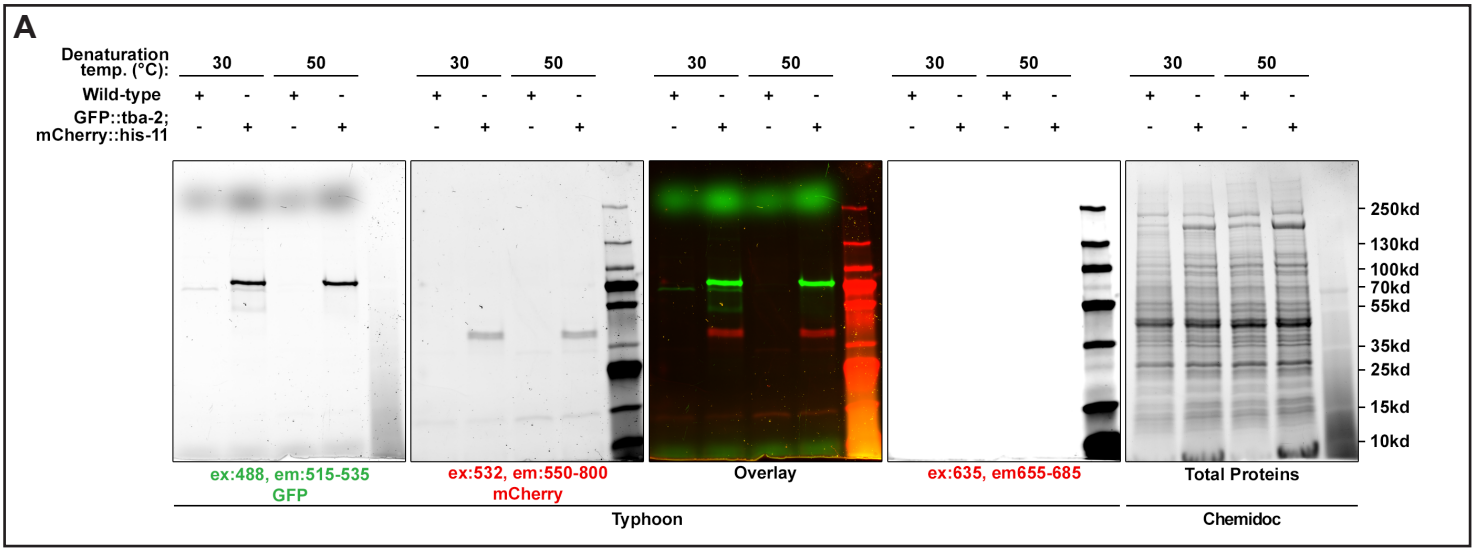
A
Denaturation temp. (°C):
30
50
Wild-type
GFP::tba-2; mCherry::his-11
250kd
130kd
100kd
70kd
55kd
35kd
25kd
15kd
10kd
ex:488, em:515-535
GFP
ex:532, em:550-800
mCherry
Overlay
ex:635, em655-685
Total Proteins
Typhoon
Chemidoc

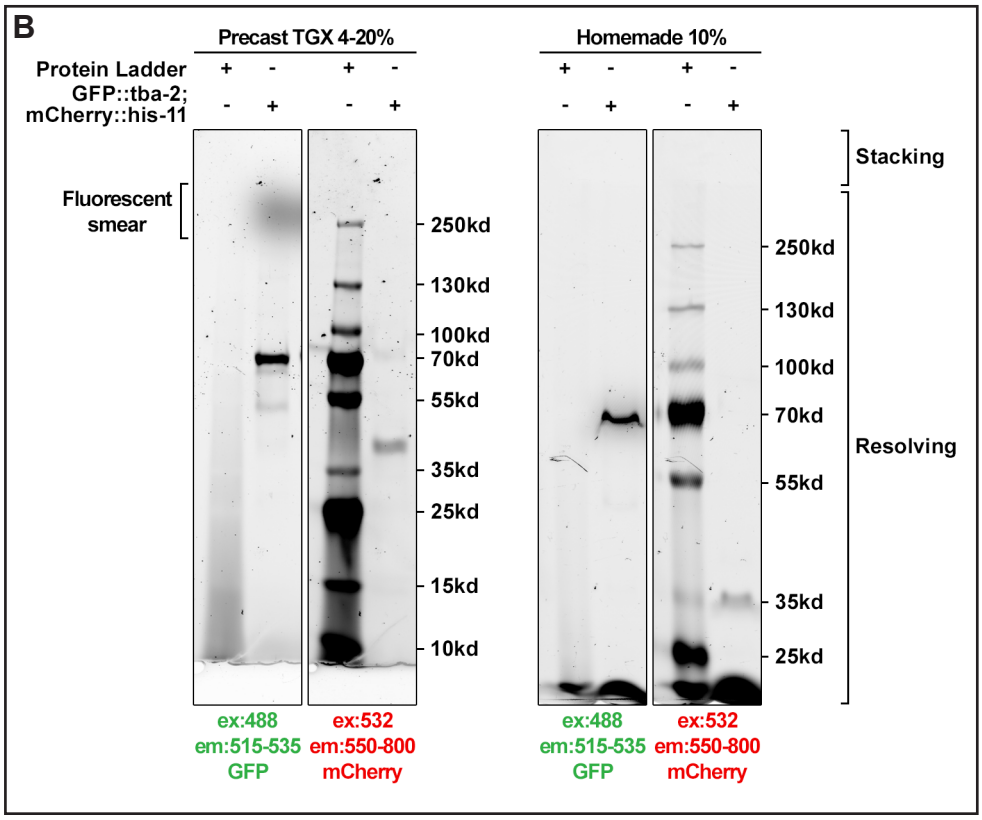
B
Precast TGX 4-20%
Homemade 10%
Protein Ladder
GFP::tba-2; mCherry::his-11
Fluorescent smear
Stacking
Resolving
250kd
130kd
100kd
70kd
55kd
35kd
25kd
15kd
10kd
ex:488
em:515-535
GFP
ex:532
em:550-800
mCherry

Figure S10